# General Disclaimer

## One or more of the Following Statements may affect this Document

FINAL REPORT ON THE ADDITION
OF EI/CI CAPABILITY TO THE
MATTAUCH-HERZOG SPECTROGRAPH WITH EOID

By G.J. Fergusson and M.E. Koslin

August 1979

# TABLE OF CONTENTS

# LIST OF ILLUSTRATIONS

# LIST OF TABLES

# 1. INTRODUCTION

A modification has been made to the Mattauch-Herzog Spectrograph with an electro-optical ion detector (EOID) previously designed and constructed for JPL, so that it would be capable of operating not only in the electron-impact (EI) mode of ionization, but also in the chemical ionization (CI) mode. This modification necessitated an effort in three specific design areas. These areas were: 1) sample inlet, 2) ion source and analyzer regions, and 3) the pumping system. In addition, an appropriate electronics package had to be designed to control and operate the combined EI/CI source.

## 2.  SYSTEM DESCRIPTION

### 2.1  VACUUM SYSTEM

In order to accommodate the increased flow of gases into the source region of the instrument due to CI, the pumping requirements for the source region and the analyzer region had to be determined.  A vacuum pumping system was then designed based on these requirements.  Project Note 1 deals with the calculation of pumping speeds for both air and methane with the chosen vacuum pumps and their associated baffles.

It was decided that the pumping system in the source region would consist of a Sargent-Welch 1402 mechanical pump (160 1/min) and a Varian VHS-4 oil diffusion pump (1250 1/sec).  In the analyzer section, a Sargent-Welch 1405 mechanical pump (60 1/min) and a Varian M-2 oil diffusion pump (175 1/sec) are used.

A new ion source housing had to be designed to mate the CI/EI source with the existing electrostatic sector housing.  The source had to be mounted on a flange to maintain easy access for maintenance.  Figure 1 illustrates the ion source-plug connections.  Table 1 lists the Ion Source-Plug-Terminal Strip Connections.  Project Note 2 describes the design of the housing, while Project Note 3 shows that the flow rate between the source region and analyzer region is 0.5%.  This indicates that the housing design has made a tight fit and is functioning properly.

In addition, an alpha stop was designed and properly located between the object slit and the electric sector to limit the angular spread of the ion beam to $\pm 1°$.

TOTAL ION MONITOR

$H^U$

HEATER

$B^U$ ◯      ◯ $D^U$

$J^L$
SOURCE BLOCK

THERMOCOUPLE

$A^U$ $E^U$
X

REPELLER ◯      ◯ REPELLER
$A^L$                    $L^L$

$F^L$
ION FOCUS

$H^L$
ION FOCUS

FILAMENT

◯      ◯
$B^L$   $D^L$
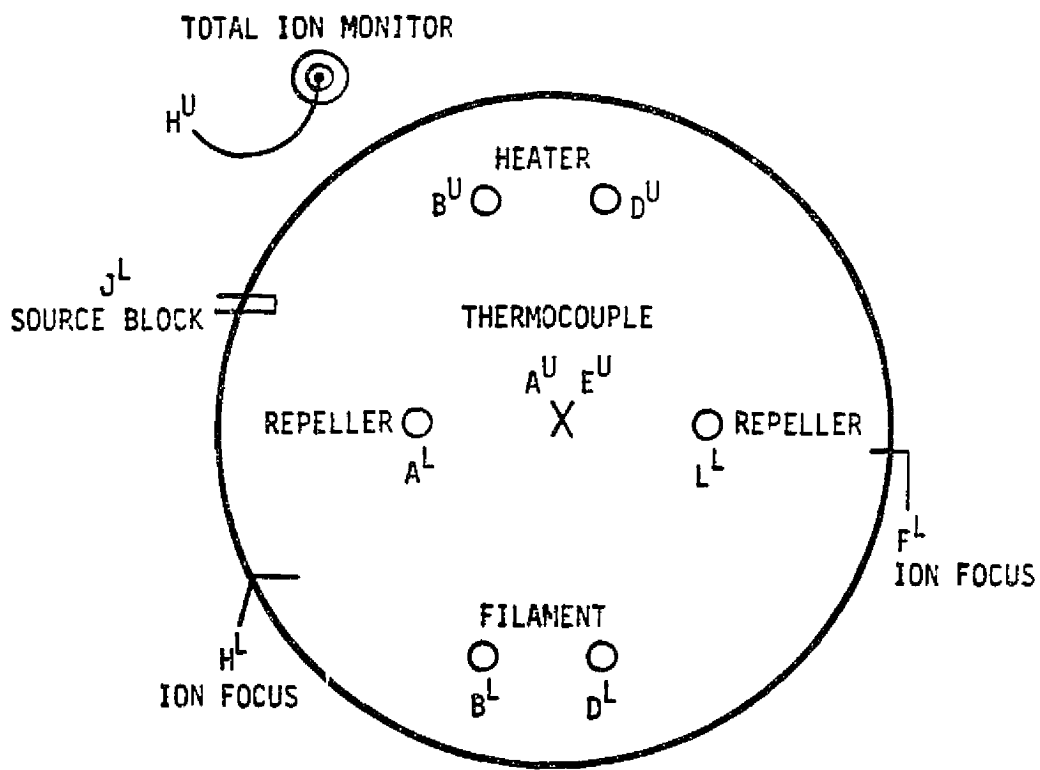
LEGEND

SUPERSCRIPT INDICATES UPPER (U) OR LOWER (L) PLUG CONNECTOR.

79-280

FIGURE 1

Ion Source-Plug Connections

-3-

## TABLE 1

## Ion Source-Plug-Terminal Strip Connections

| Source Connection | Plug Connector | Terminal Strip Connection |
|---|---|---|
| **UPPER PLUG** | | |
| Source Block Heater | D | None |
| Source Block Heater | B | None |
| Thermocouple | A | None |
| Thermocouple | E | None |
| Total Ion Monitor at Alpha Stop and Ground | H | 11 |
| **BOTTOM PLUG** | | |
| Filament | B | 1 |
| Filament | D | 2 |
| Left Repeller | A | 3 |
| Right Repeller | L | 4 |
| Source Block | J | 5 |
| Right Ion Focus | F | 6 |
| Left Ion Focus | H | 7 |
| Negative Z-Axis | None | 8 |
| Positive Z-Axis | None | 9 |
| Positive ESA | None | 10 |
| Negative ESA | None | 12 |

## 2.2   INLET SYSTEM

To accommodate the introduction of reagent gases for CI, a new sample inlet
system was designed.  This system had to be capable of not only allowing flow
of 2 atm cc/min for CI operation but also of being switched to a region where
a flow splitting of 20:1 occurs so that EI conditions prevail.  The inlet
system would also have to be insulated from the source block so a gaseous
discharge would not occur from the source block which is at a high potential
of ca. 1300 V.  Project Note 4 describes the design of the inlet system and
Project Note 5 details the testing procedure involved with designing the
insulating technique for the gas inlet line.

The inlet system was designed to have a thermal zone with a temperature of
200°C controlled to ±10°C.

## 2.3   DETECTION SYSTEM

The detection system for this instrument consists of five microchannel plates
in series along the focal plane of the mass spectrometer.  These microchannel
plates have been supplied by JPL and were fabricated by Galileo Electro-
Optics Corporation.  The microchannel array (MCA) produces efficient conversion
of the incoming ions to secondary electrons and causes further secondary
electron multiplicaton, yielding a gain of $10^3$.  The electrons are then
accelerated and allowed to strike a phosphor.  The intensity of the image
formed on the phosphor is proportional to the number of ions striking the
MCA.  In the present arrangement, the image intensity is measured by a Gamma
Scientific Photometric Microscope, Photo Multiplier, and Digital Photometer.
The calibration of the detector was discussed in Project Note 18 in the Final
Report for Contract No. NAS7-100.

The output of the digital photometer was fed to the input of an X-Y Recorder
or a time-based Strip Chart Recorder.  It was possible to obtain a complete
recording of the mass spectra by moving the photometric microscope along the
focal plane and displaying the output on the strip chart recorder producing
a mechanical scan of the spectra.  If a very small segment of the spectra is

needed to be displayed, the photometric detector is positioned and the accelerating potential scanned from V(ACC) to V(ACC) ±100 V. The output from this voltage scan was displayed on the X-Y Recorder. Because of this recording scheme, it was necessary to have a continuous production of the mass spectra. Thus, it was not possible to utilize a gas chromatograph for sample introduction as a steady state sample would not be available.
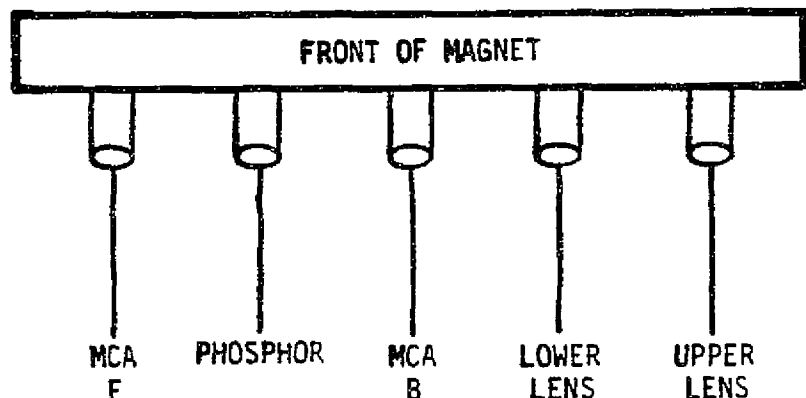
In addition to the detection system described above, the capability of utilizing post-focus ion acceleration (PFIA) has been designed for the exit region of the magnetic sector. The purpose of the PFIA is to give the ions sufficient additional energy (beyond that obtained from the accelerating potential) to increase the yield of the MCA, resulting in an increase of S/N. Figures 2 and 3 illustrate the electrical connections for the electro-optical ion detector (EOID) and the schematics for the electrical connections for NON-PFIA and with PFIA.

## 2.4  ELECTRONICS

The electronics package developed for this instrument has three primary functions. These are: 1) to supply all voltages to the CI/EI ion source, 2) to provide means to control the temperature of the inlet and ion source, and 3) to provide power for the vacuum system. In addition, protective circuitry and voltage scanning are provided for some systems. Figure 4 is the source control panel layout while Figure 5 is the schematic of circuitry which supplies power for: the filament, for emission regulation, potentials for ion acceleration, repellers, ion focus plates, Z-axis lens and the electrostatic analyzer. To protect the filament, the filament power supply will not operate unless the accelerating voltage is greater than 500 volts.

As previously mentioned, scanning the mass spectra over a range of 100 volts by a continuous voltage ramp is achieved by a circuit illustrated in Figure 6.

Temperature control for the source block and inlet systems is achieved by thermocouples in each area and a Wolfe Industries Temperature Controller Style 303K regulates the temperature at 200°C ±10°C.

FRONT OF MAGNET

MCA
F  PHOSPHOR  MCA
B  LOWER
LENS  UPPER
LENS

79-279

FIGURE 2

EOID Connections



NON-PFIA

MCA

UPPER LENS

PHOSPHOR

+3900

LOWER LENS

+1000

PFIA

-800 -1200

UPPER LENS

PHOSPHOR

+2900

LOWER LENS

-800 -1200

-1000

MCA
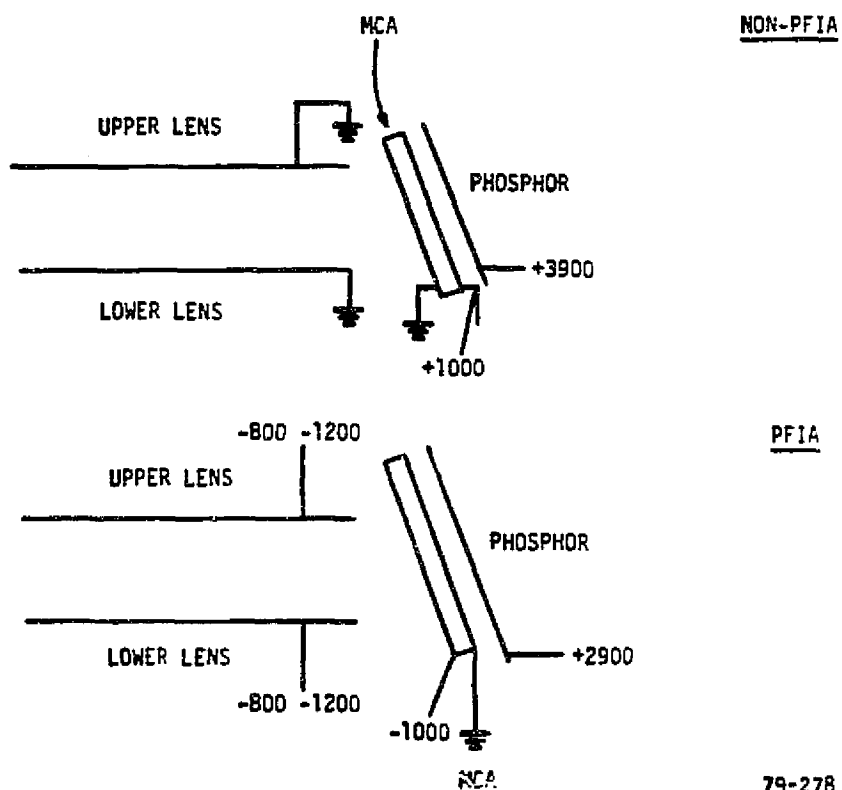
79-278

FIGURE 3

Electrical Connections for EOID
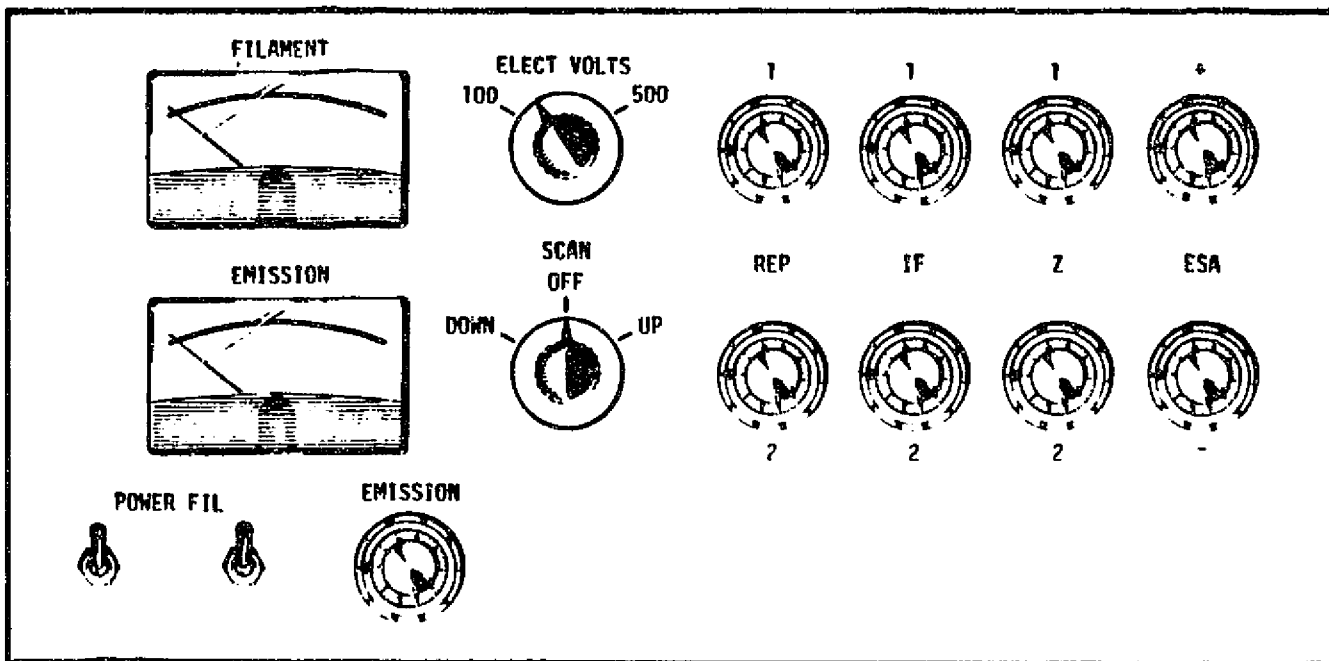
FIGURE 4

Source Control Panel Layout
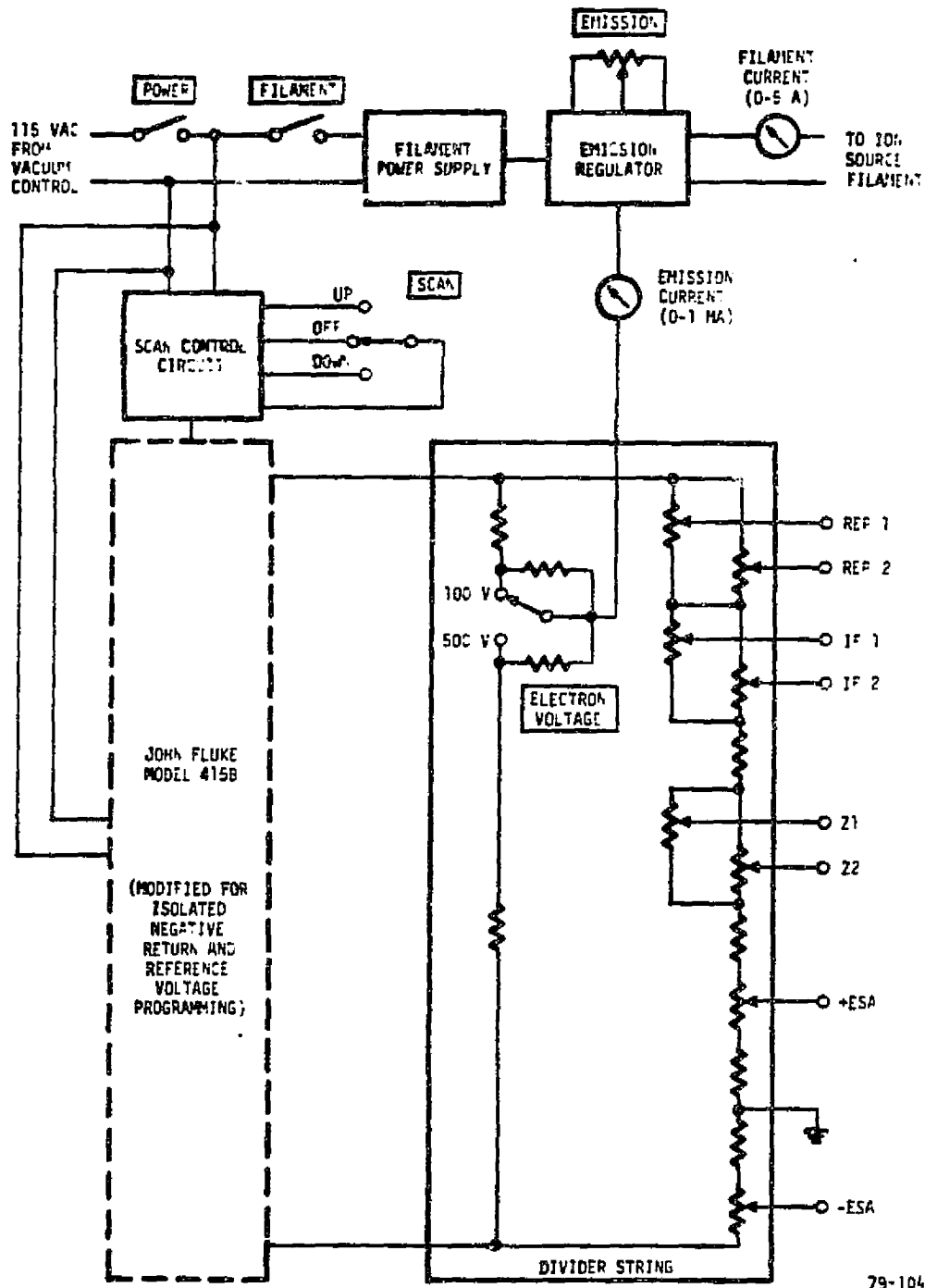
FIGURE 5

Source Control Panel Block Diagram
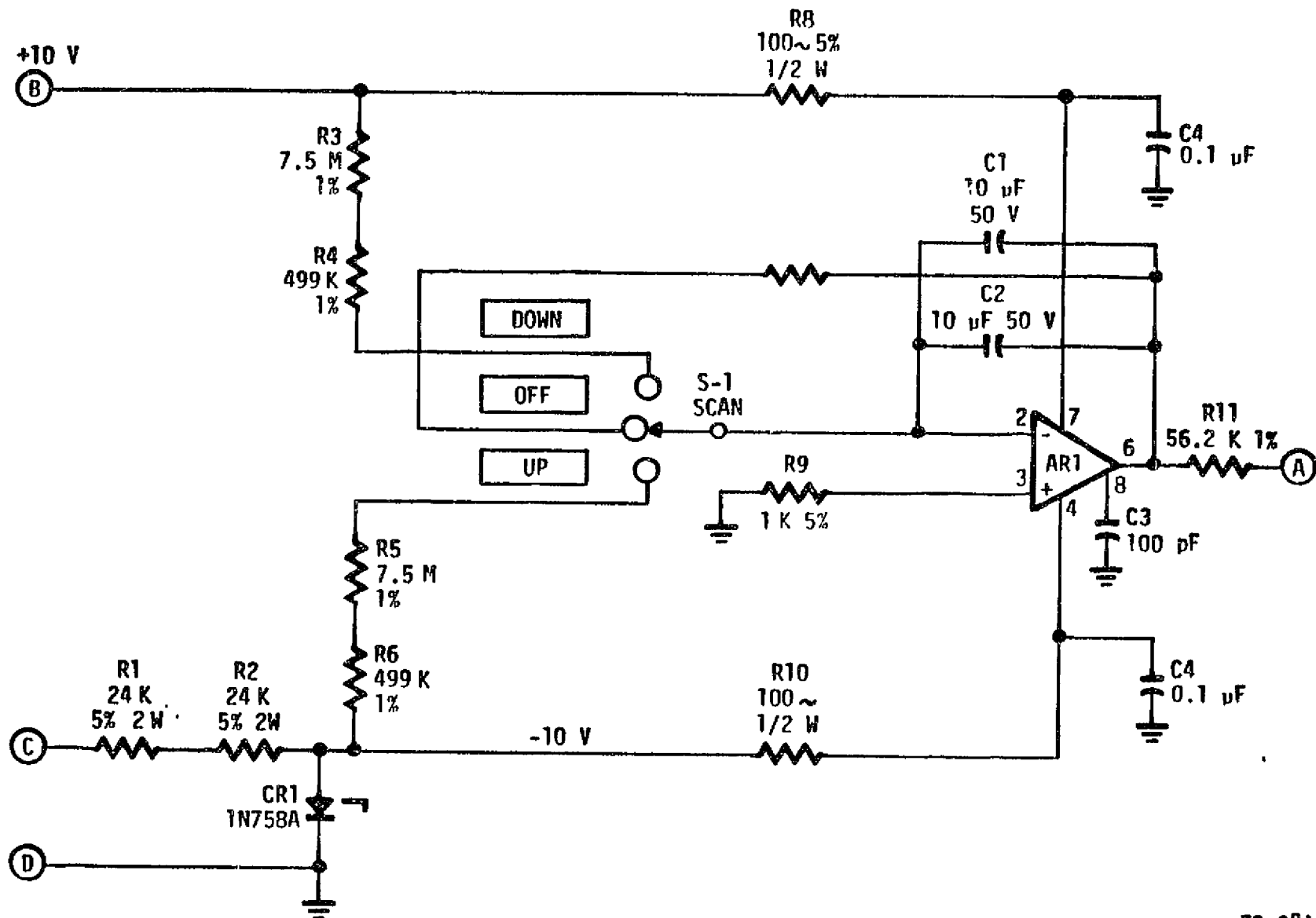
FIGURE 6

High Voltage Scan Circuit for Fluke 412B HVPS

79-281

Figure 7 is the schematic for the wiring to provide power to the mechanical pumps, diffusion pumps, and to the electronics package. Additionally, there is a pressure sensitive water flow switch in the circuit to the diffusion pumps. In the event the flow decreases and adequate cooling is not provided for the diffusion pumps, power is cut off to the pumps.

## 2.5 NORMAL OPERATING VALUES

To provide for a reproducible experimental environment, the following values of operating parameters were normally used: accelerating potential, V(SB): 1500 volts; phosphor voltage: 3900 volts, and the voltage to the MCA: 1000 volts. Table 2 lists the voltage range available for the ion source potentials and focusing parameters.
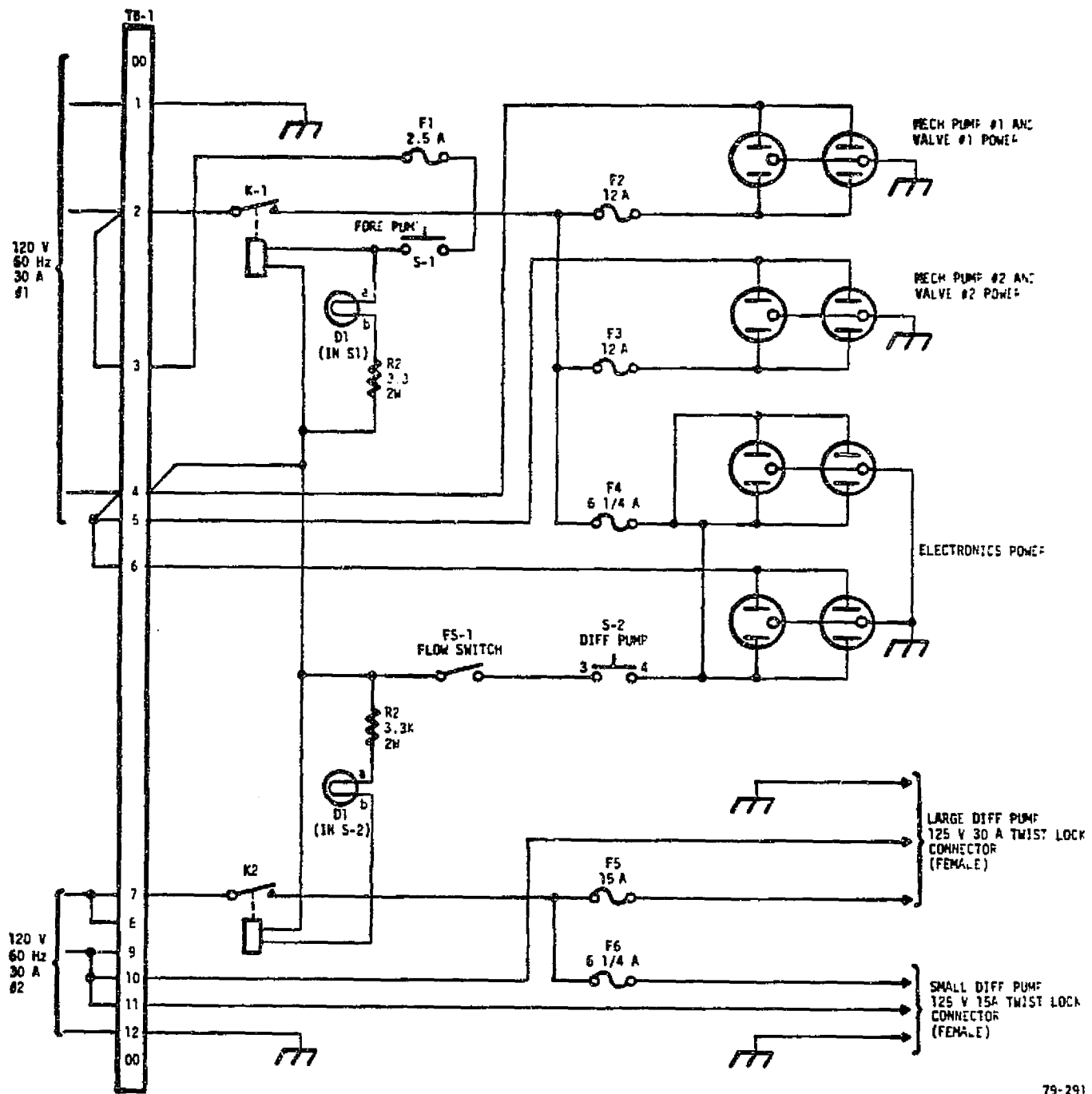
**FIGURE 7**

**Schematic for Power Wiring**

79-291

-12-

## TABLE 2

### Ion Focusing Parameter Voltage Range

| <u>Parameter</u> | <u>Range</u> |
|---|---|
| Repeller No. 1 and 2 | 1400 - 1422 |
| Source Block | 1400 |
| Ion Focus No. 1 and 2 | 1292 - 1400 |
| Z-Axis Lens | 345 → 560 |
| Positive ESA | 86 → 108 |
| Negative ESA | -86 → -108 |

# 3.   EXPERIMENTAL RESULTS

## 3.1   EOID CHARACTERIZATION

Since all of the spectral information generated in this instrument was
obtained by the conversion of ions to secondary electrons in the MCA, it
was very important to have the MCA well characterized.  For this purpose,
two experiments were initially performed.  The first experiment determined
the peak intensity as a function of ion accelerating voltage.  The voltage
range selected was from 1000 to 2000 V for ions of m/e 131.  Both voltage and
mechanical scans were made of the same mass peak for several accelerating
potentials.  Figures 8 and 9 show the voltage and mechanical scans respec-
tively.  It is apparent that the experimental points do not show a smooth
curve for the relationship between intensity and accelerating voltage, which
would indicate that the MCA does not yield a uniform gain across its surface.
This was confirmed in a separate experiment where the sensitivity was measured
along the MCA plane.  A mass peak equivalent to m/e 381 was moved along the
MCA by a slight change in the accelerating potential.  The photometric micro-
scope was then repositioned and a voltage scan was recorded.  Figure 10
illustrates the variation of the sensitivity along just 0.100 inch of the MCA.
Within this length one measures a sensitivity variation by a factor 3.5.  This
indicates that no quantitative information should be obtained from a mechanical
scan of the MCA plane, as the gain is not uniform.  Quantitative information
can more reliably be accomplished by voltage scanning.  The reason for this
is that the area of the MCA used during analysis via voltage scanning is kept
constant.  Thus the gain in the MCA is also constant.

Another quantity measured during the experimental stage was the rotation of
the image as a function of the voltage applied to the EOID.  Figure 11 illus-
trates the variation of the peak intensity, peak integral, and the image
angle for m/e 381 ions as a function of applied voltage to the phosphor.

-14-
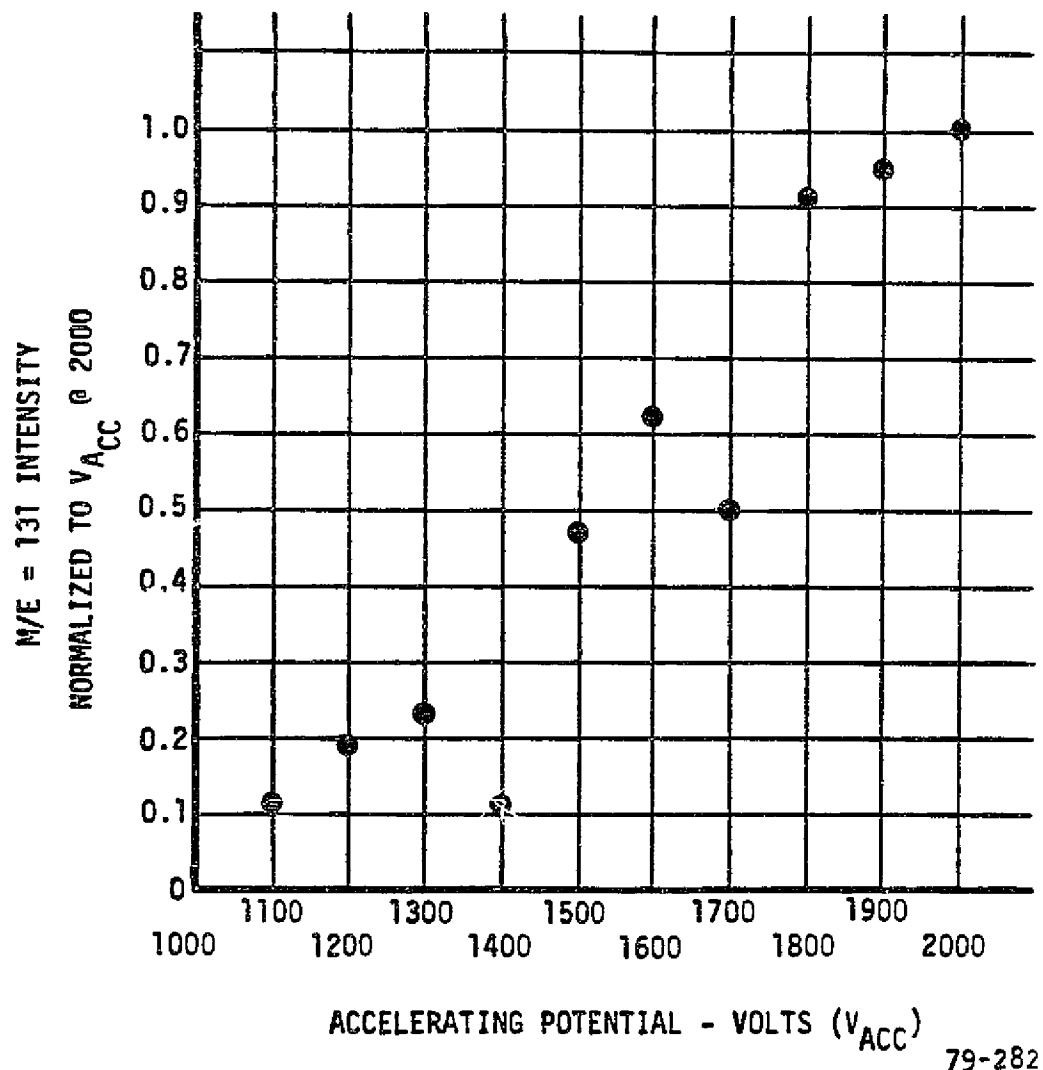
FIGURE 8

Peak Intensity vs Accelerating Potential-Voltage Scan
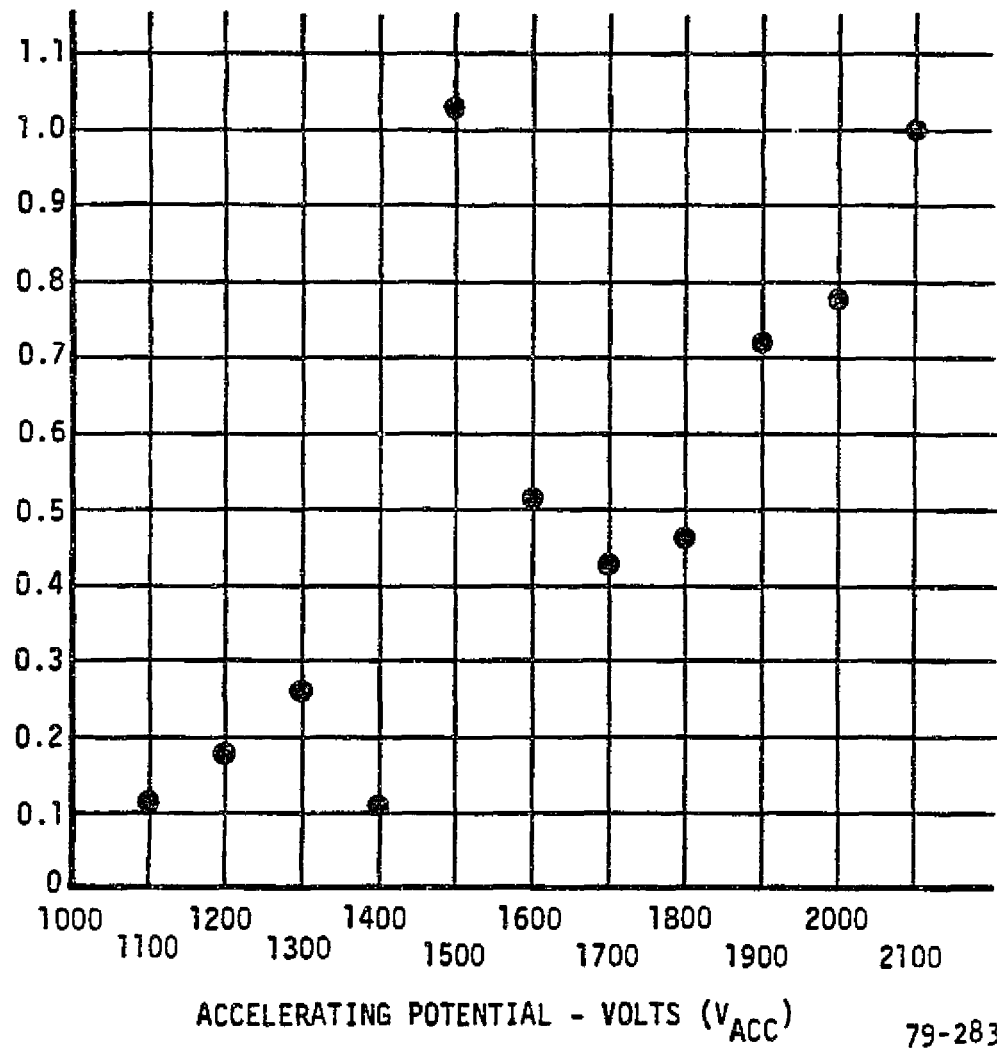
FIGURE 9

Peak Intensity vs Accelerating Potential-Mechanical Scans
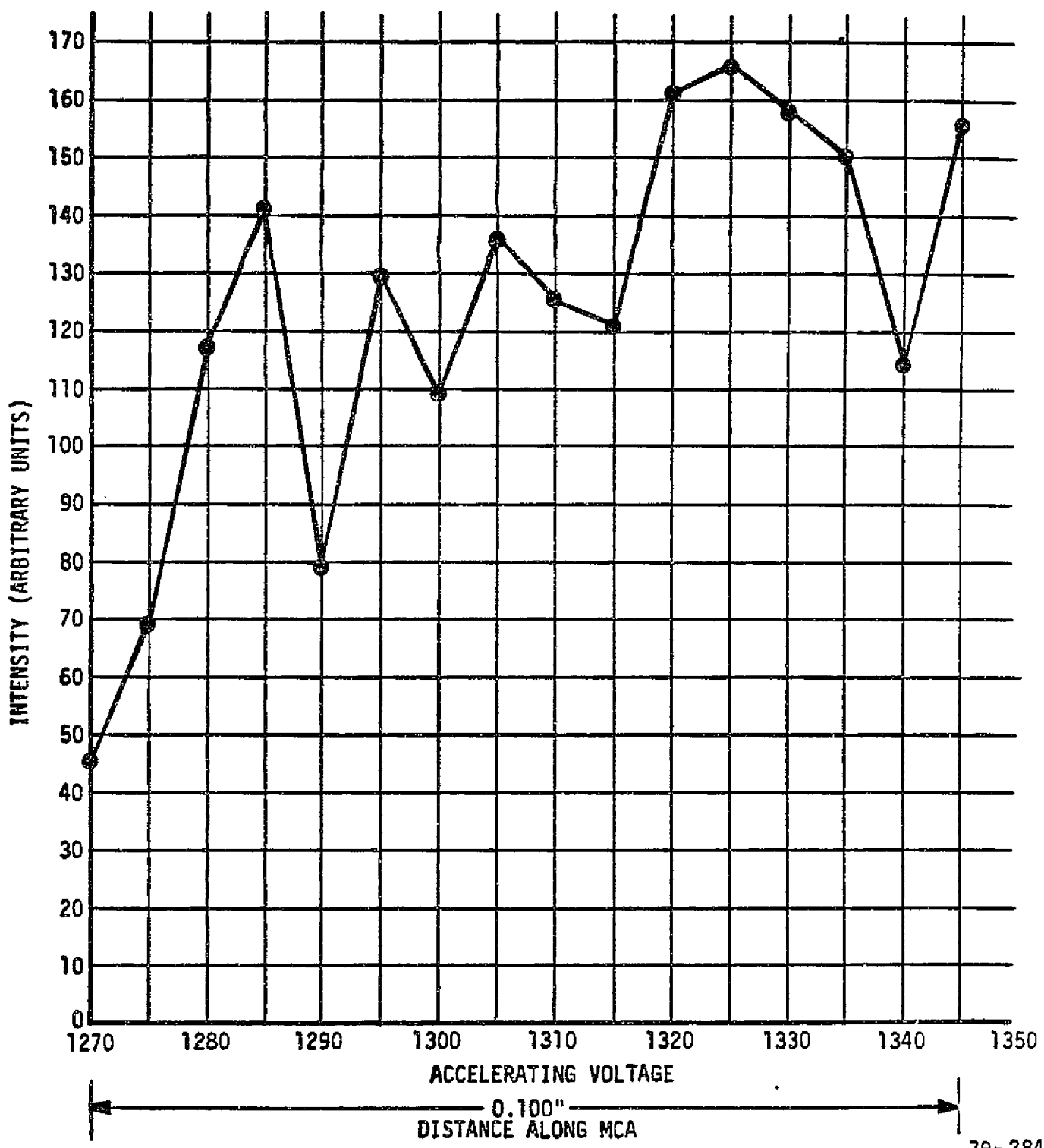
**FIGURE 10**

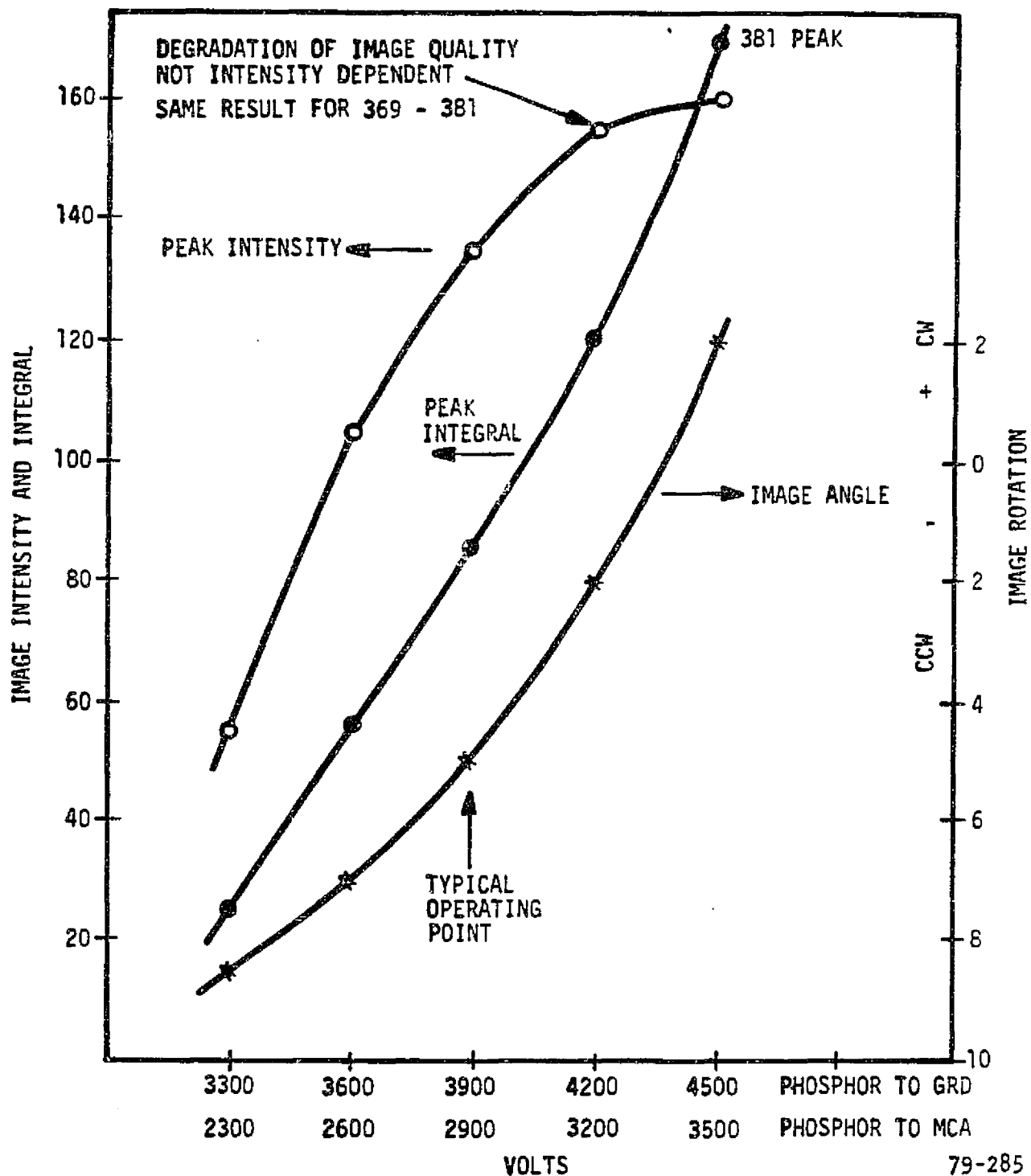Variation of Sensitivity Along MCA Plane

79-284

-17-

**FIGURE 11**

Variation of Image Quality as a Function of Phosphor Voltage

There is an image rotation of 10 degrees when the applied voltage between the phosphor and the MCA is changed 1200 volts. The image angle is important for the fabrication of the fiber optics which will be used to transfer the image out of the EOID as it will have to be rotated to the corresponding angle. Figure 12 represents the image position as a function of the potential difference between the MCA and the phosphor. It appears that as the potential difference increases, the image height also increases slightly.

## 3.2  MAGNET POSITIONING

Due to addition of the CI/EI source, the entire instrument had to be disassembled. After reassembly, the optimum position for the magnet had to be experimentally determined. To achieve correct positioning, perflurokerosene (PFK) was introduced into the system and mass peak 381 was located. Voltage scans of this mass peak were obtained at various magnet positions and the full width at half maximum (FWHM) was determined. Figure 13, shows the results of plotting the FWHM vs magnet position. A similar plot, shown in Figure 14, was made of the same peak under the conditions of PFIA. It is apparent that the optimum position (the position which results in the minimum FWHM) occurs at a position of approximately .150 inch without PFIA and at .175 inch under the conditions of PFIA. These positions are expressed relative to a fully forward position.

## 3.3  Z-AXIS LENS EFFECT ON TRANSMISSION

After the proper magnet position had been found, it was useful to determine the effect of the Z-axis lens on ion transmission. For this purpose, perflurobutene (PFB) was introduced into the ion source to give a pressure of $10^{-6}$ torr in the source housing. An EI spectra was determined with an electron beam emission current of 0.15 mA at 1500 volts ion accelerating potential. The photometric microscope was set to monitor the peak corresponding to m/e 181.

The intensity of the m/e 181 peak was measured with an applied voltage and ground potential to the lens. When at ground, refocusing of the image was
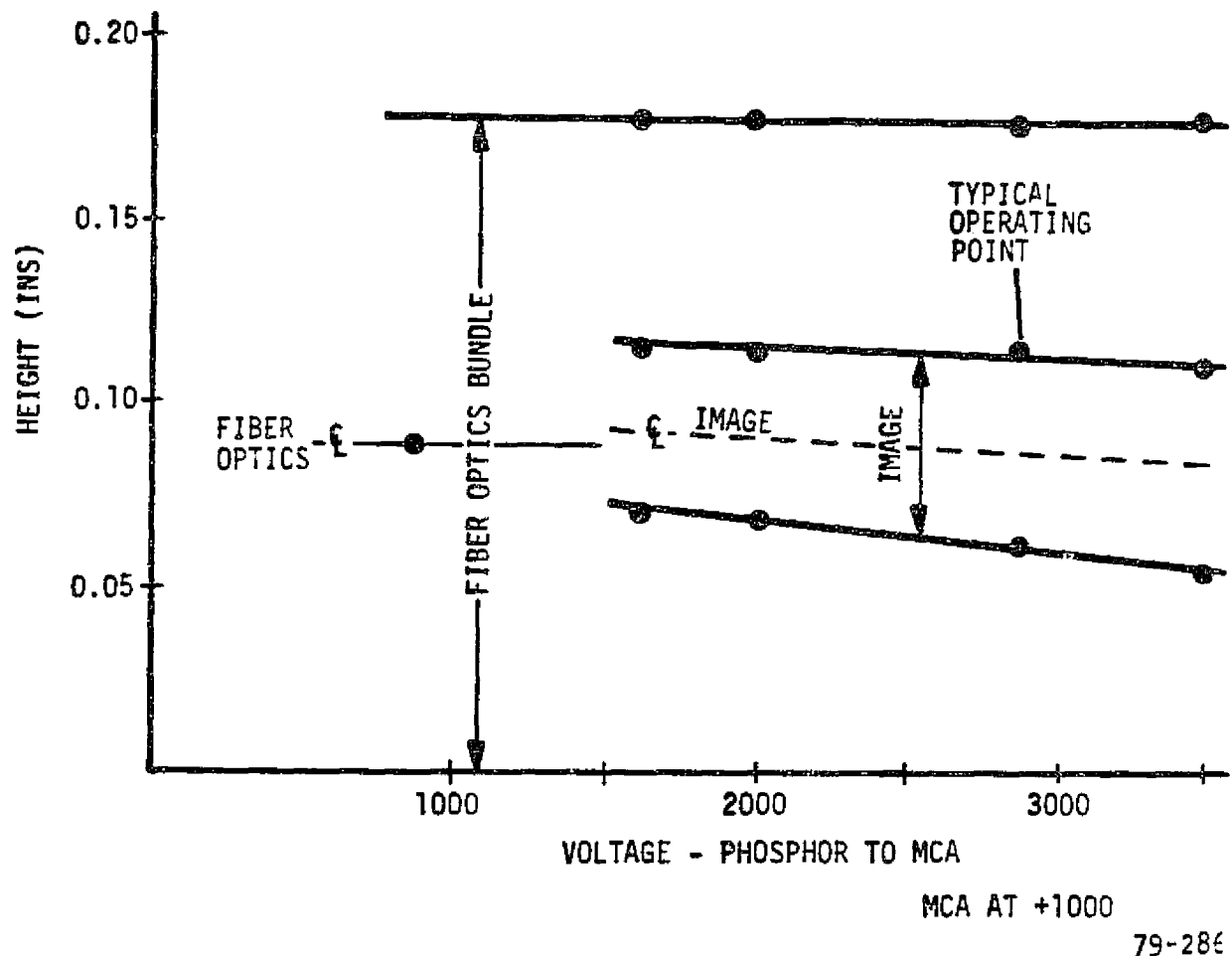
FIGURE 12

Image Position – Fiber Optics Output
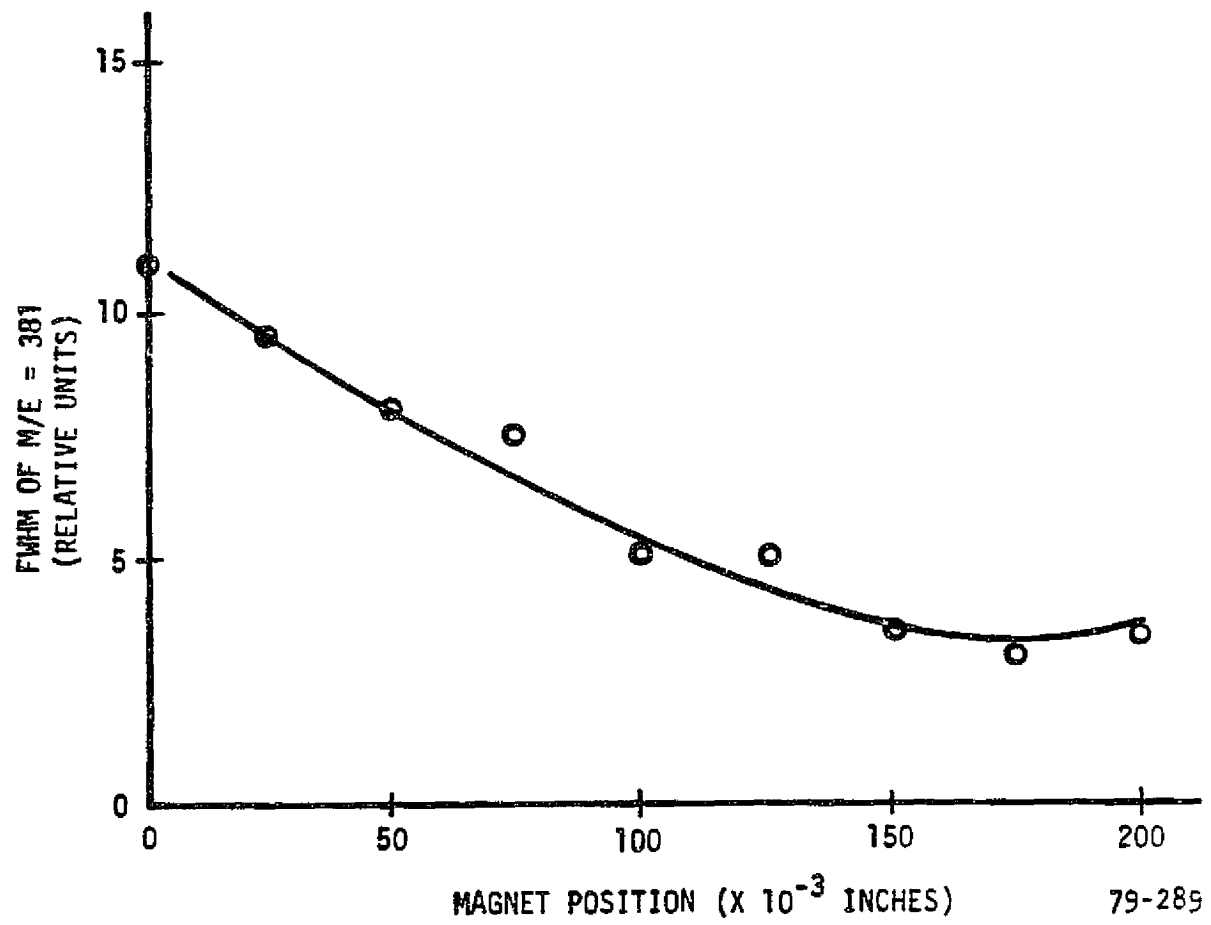
FIGURE 13

Peak Width vs Magnet Position Non-PFIA
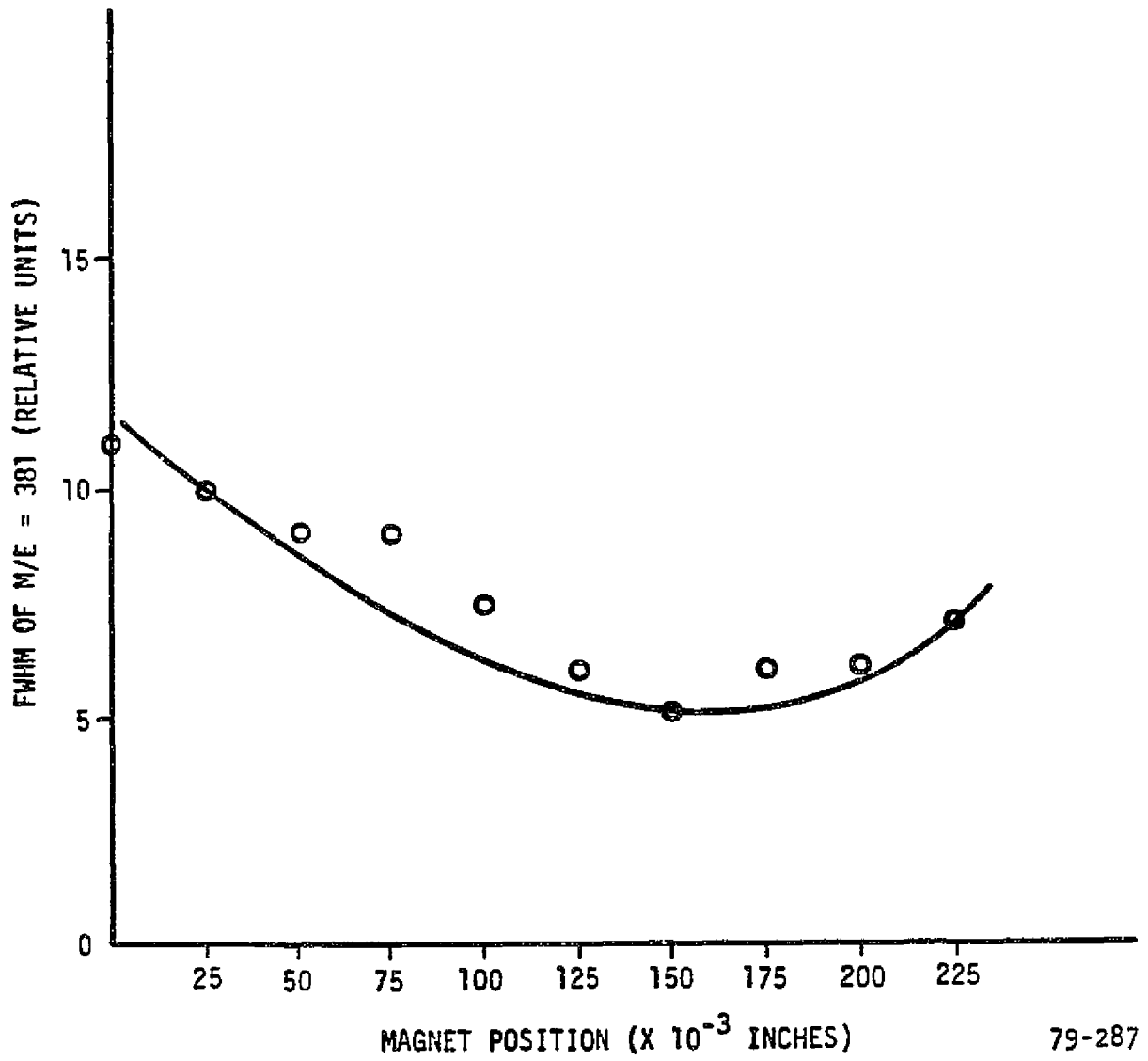
FIGURE 14

Peak Width vs Magnet Position With PFIA

79-287

-22-

necessary. Figure 15 illustrates the image itensity of the m/e 181 peak both with and without applied voltage as well as with voltage and mechanical scans.

The improvement of the ion transmission due to the Z-axis lens potential was almost four using both mechanical and voltage scans.

## 3.4 RESOLUTION

From early experiments, it became evident that possibly a skewing of the magnet had occurred during reassembly, resulting in misalignment of the ion and MCA focal planes. This meant that different values of ESA potential would be needed to achieve optimum resolution for different masses. To select compounds which produced sizable mass peaks for resolution measurement, freon C318, PFB, PFK, and penthrane were used. These compounds have base peaks ranging from m/e 200 to m/e 400.

## 3.5 FREON C318

Freon C318 was introduced into the system to give a pressure of $4.7 \times 10^{-6}$ torr in the source housing. A mass spectrum of this compound is shown in Figure 16. Figure 17 is a voltage scan of the m/e 131 peak. The resolution at this point is 149.

## 3.6 PERFLUOROBUTENE-2

Perfluorobutene was introduced in the system in order to obtain an EI and CI spectra utilizing methane as the reagent gas. This was a particularly useful sample as it produced the same mass range as the freon C318 enabling easier mass identification. Figures 18 and 19 represent mass scans of PFB under EI and CI conditions respectively. As one can see, the methane has caused an increase in the sensitivity for groups of ions with m/e approximately 181, 160, and 140 and a decrease in sensitivity to m/e 131, 150 and other middle mass peaks.

-23-
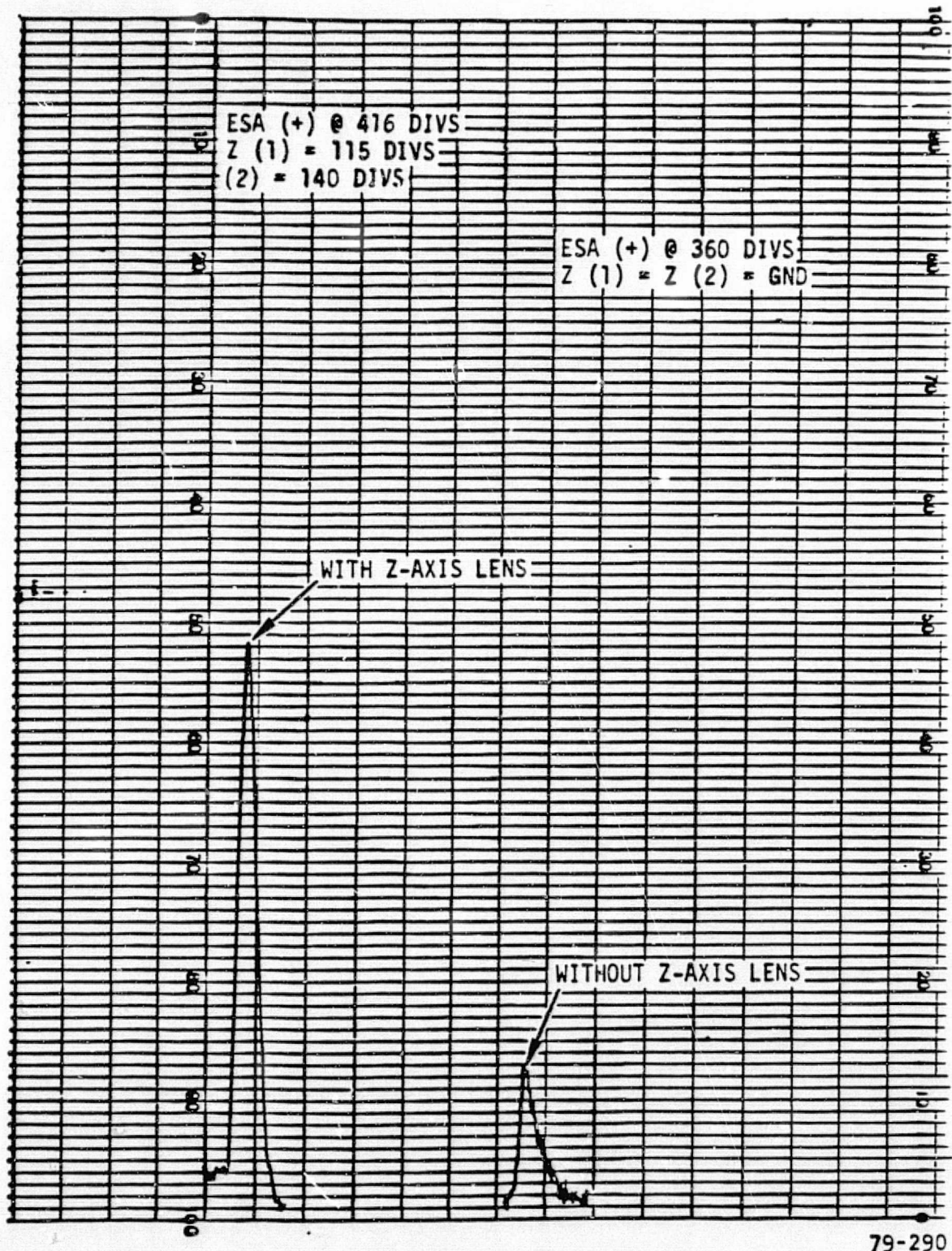
**FIGURE 15**

Effect of Z-Axis Lens on Image Intensity

79-290

FIGURE 16

Freon C318

$P_S = 4.7 \times 10^{-6}$

$V_{SB} = 1800$

$V_{PH} = 3430$

$V_{MCA} = 1000$

$I_e = 0.1$ mA

INPUT = 50 mV

NOTE: MAXIMIZED HIGH MASS END

1491  TOPPED OUT

$P_S = 1.6 \times 10^{-5}$ TORR
$V_{PH} = 3850$
$V_{MCA} = 1000$

V = 1480

132      131
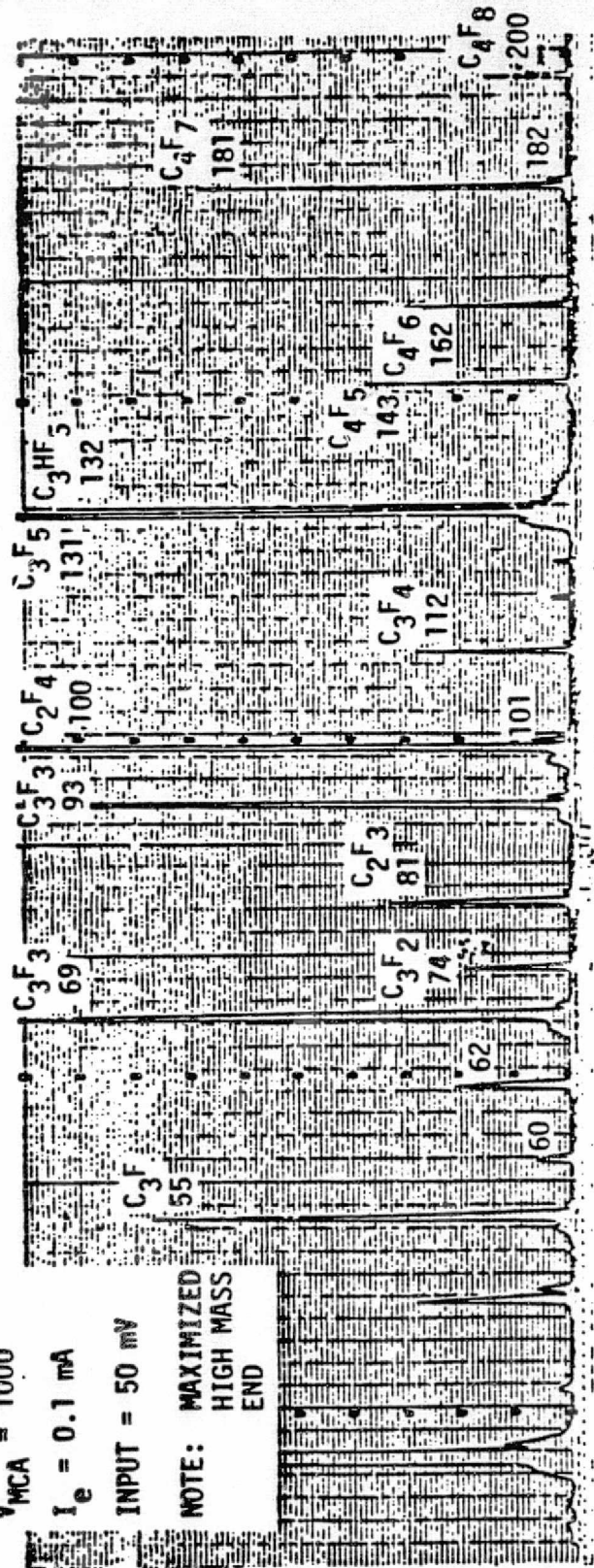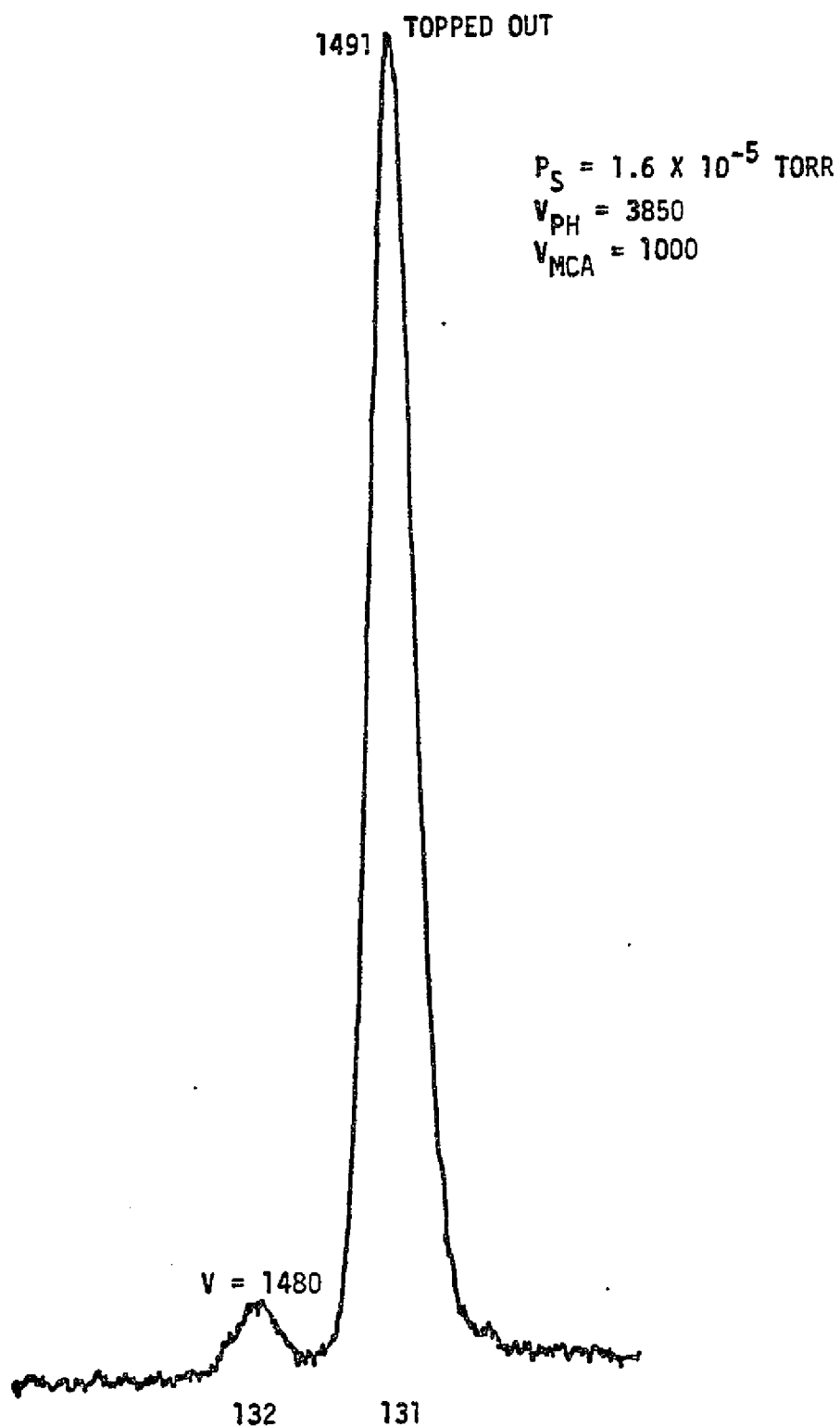
FIGURE 17

Freon C318

-27-

ESA (+) = 185

(−) = 475

Z (1) = 409

(2) = 376

IP (1) = 114

(2) = 153

REP (1) = 571

(2) = 795

$V$ ($\overline{SB}$) = 1500

$P_S$ = 4.2 X $10^{-6}$

$P_A$ = 2 X $10^{-7}$

INPUT = 0.14

$I$ ($\overline{e}$) = 0.18
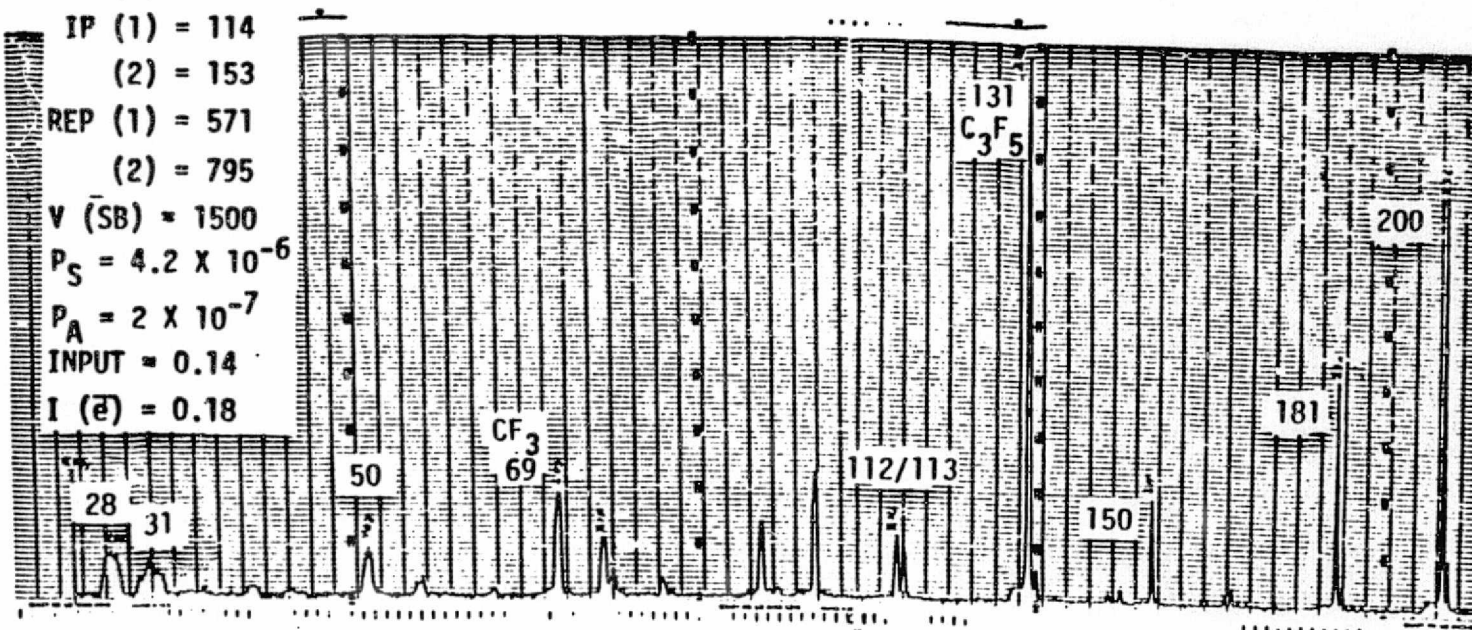
28

31

50

$CF_3$
69

112/113

131
$C_3F_5$

150

181

200

FIGURE 18

PFB
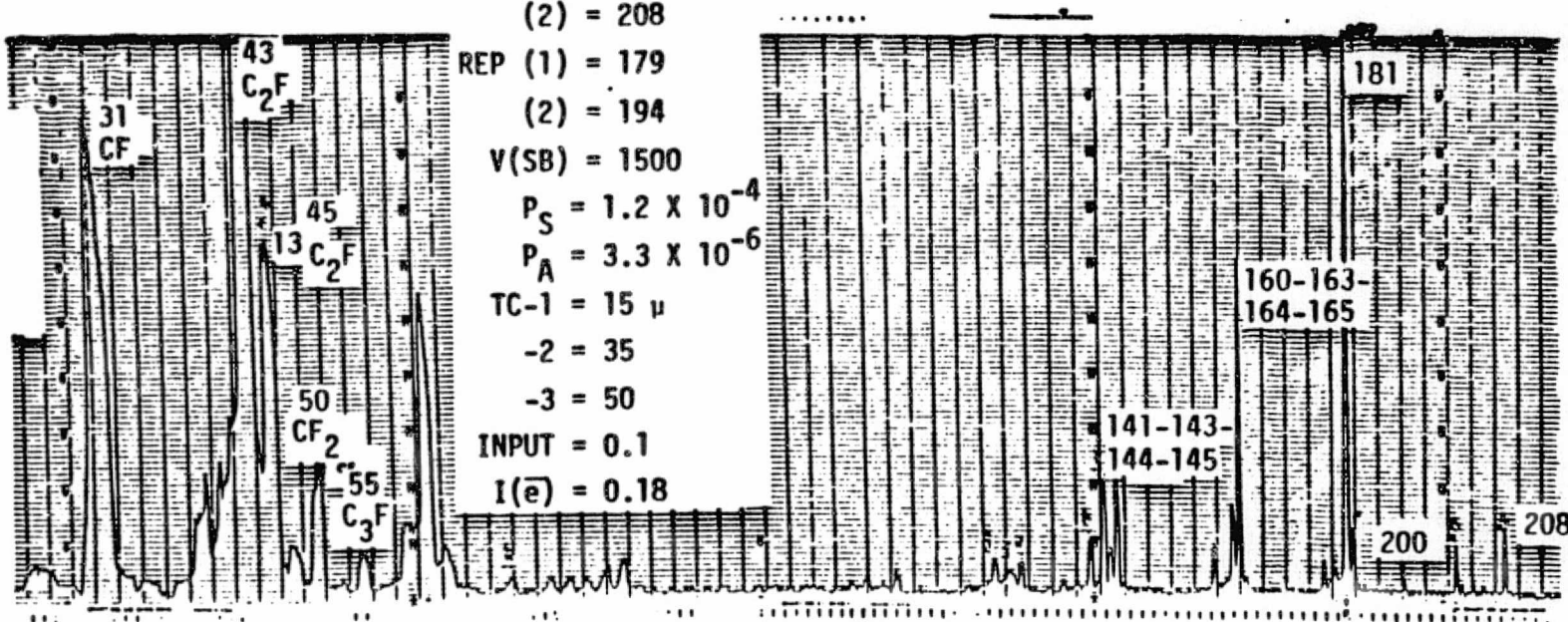
FIGURE 19

PFB With $CH_4$

Figure 20 illustrates the resolution obtained for m/e 181 in both the EI mode (R = 339) and the CI mode (R = 226).

## 3.7 PERFLUOROKEROSENE

It was then determined to extend the mass range of our sample to approximately m/e 400. For this purpose, PFK was introduced into the system and tested under PFIA conditions.

Figure 21 illustrates a mass spectrum of the peaks m/e 381 and 382 under conditions of no PFIA. The measured resolution was 572. Under PFIA conditions a mass spectrum for the range m/e 381-400 was taken with the resulting resolution dramatically reduced to 237. This is shown in Figure 22. This decrease in resolution is due to the fact that PFIA causes the ion image to distort into the shape of a comma. Since the photometer detector merely integrates the vertical projection of the image in its path, the output is a broadened image.

## 3.8 PENTHRANE

Penthrane was introduced into the system to see if a better CI spectra could be obtained with methane as a reagent gas with a nonfluorinated compound. Figures 23 and 24 represent a portion of the penthrane mass spectrum in the range m/e 129-133, in the EI and CI mode, respectively. The resolution at m/e 129 in the EI mode was determined to be 214 and in CI was 205. Table 3 lists the resolution of four mass peaks in both the EI and CI modes. These four masses cover over one half of the mass spectrum. In all cases, the CI mode gave essentially the same spectrum and resolution already obtained in the EI mode of ionization. This raised the question of whether or not true spectra were obtained under ideal CI conditions.

## 3.9 DETERMINATION OF OBJECT SLIT WIDTH

Prior to disassembly of the instrument for the conversion to the EI/CI source, the best resolution that was obtained at mass 381 is shown in Figure 25. The

EI MODE
M/E = 181
R = 339

CI MODE
M/E = 181
R = 226

179

182

FIGURE 20

PFB-2

381
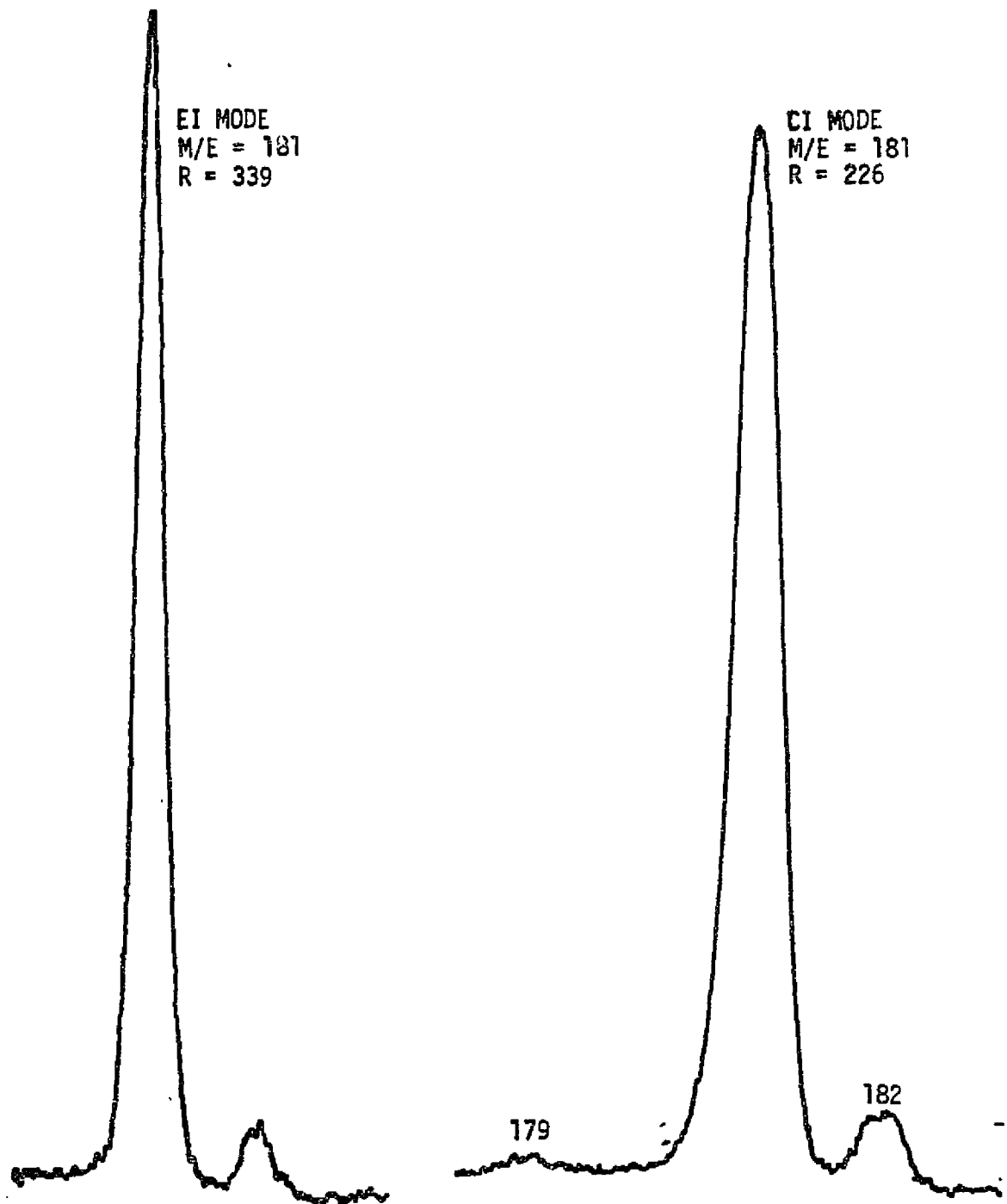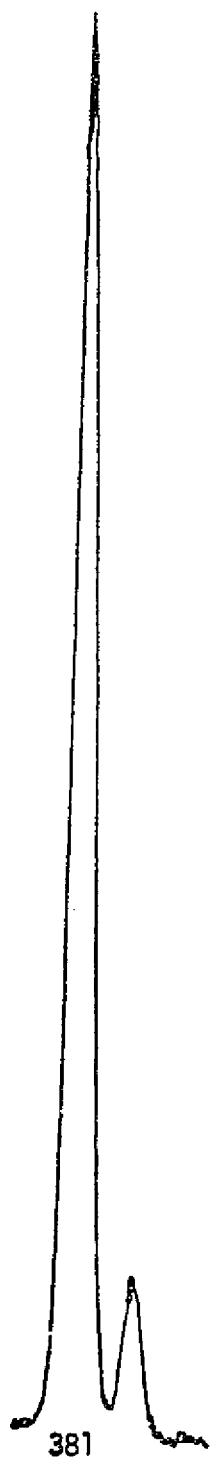
FIGURE 21

PFK Without PFIA
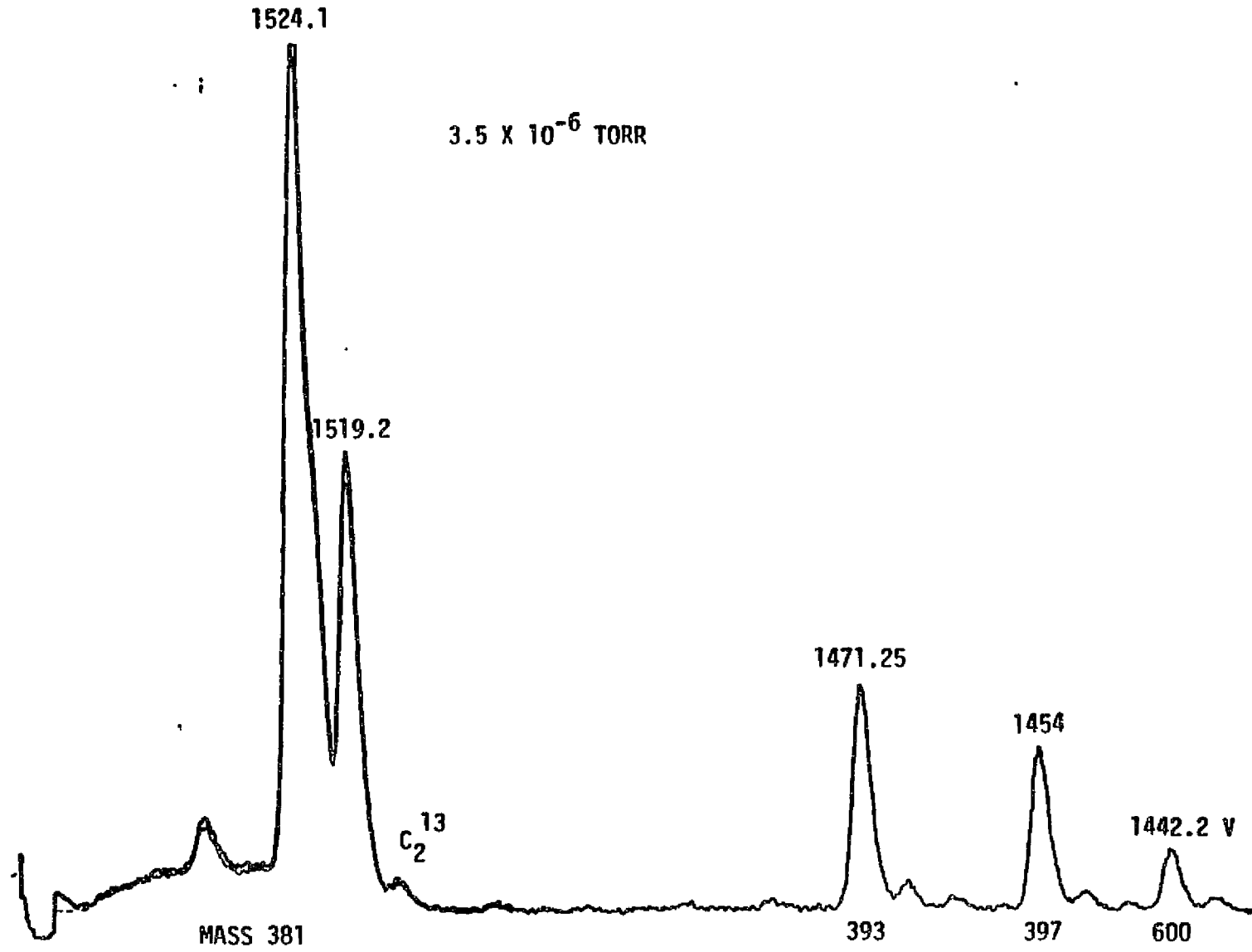
FIGURE 22

PFK With PFIA
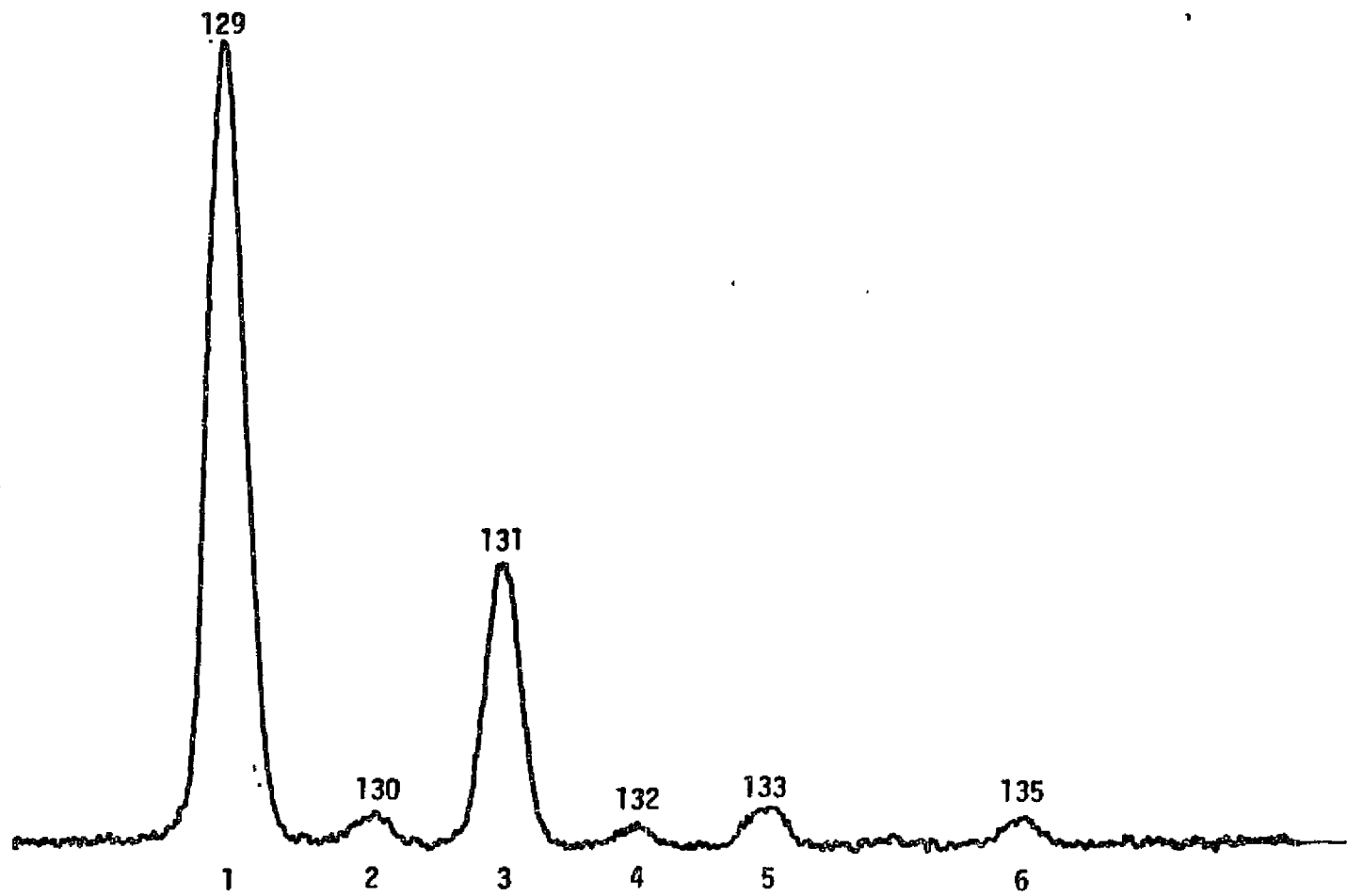
FIGURE 23

Penthrane — EI Mode
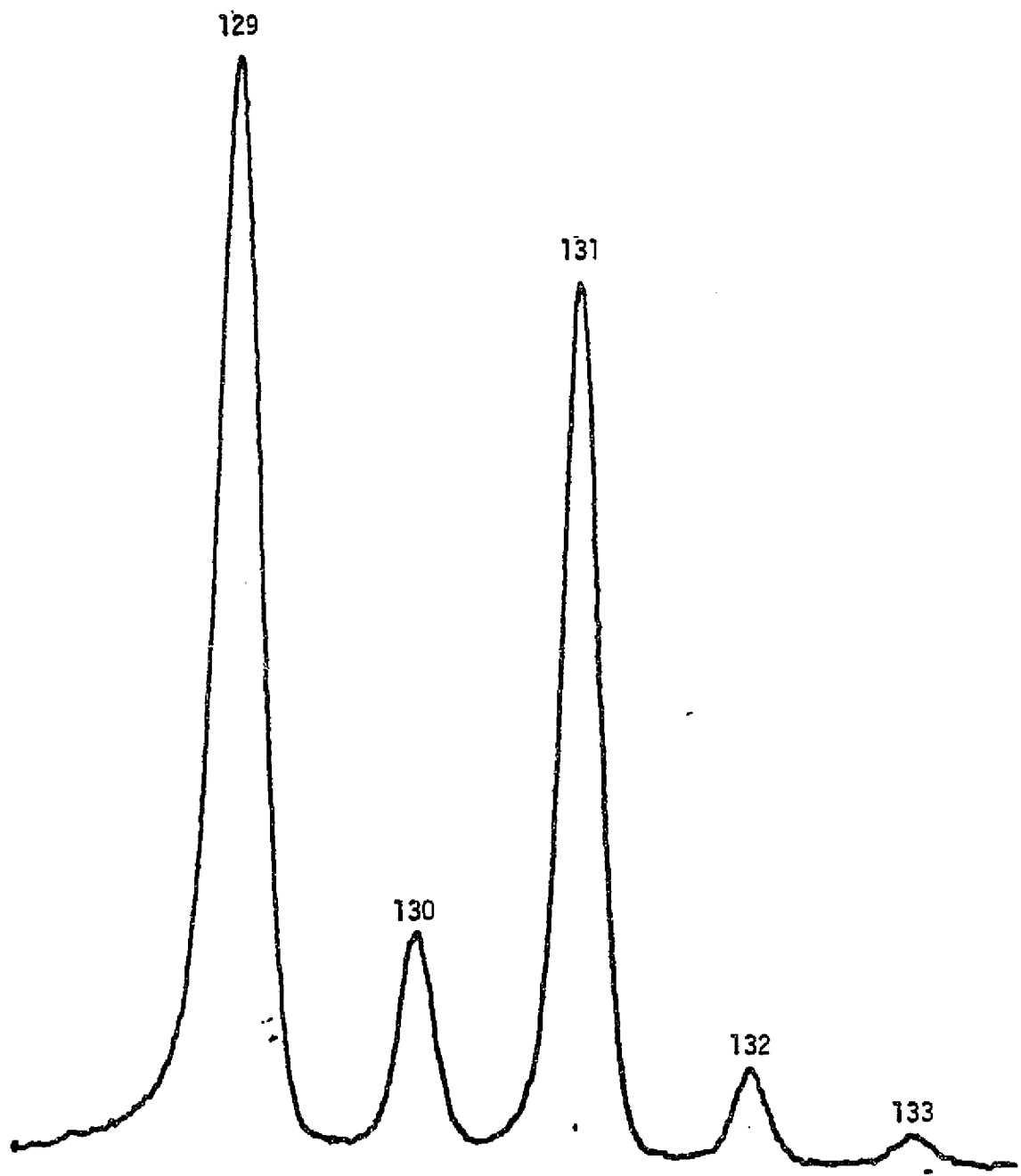
FIGURE 24

Penthrane – CI Mode

## TABLE 3

### Resolution of Various Mass Positions in Penthrane

| Mass Number | Resolution | |
|:---:|:---:|:---:|
| | EI | CI |
| 83 | 179 | 157 |
| 129 | 214 | 205 |
| 145 | 243 | 195 |
| 180 | 294 | 327 |

NO EMISSION

GATE CLOSED

$$R = 381 \times \frac{8.5}{7.5} = 431$$
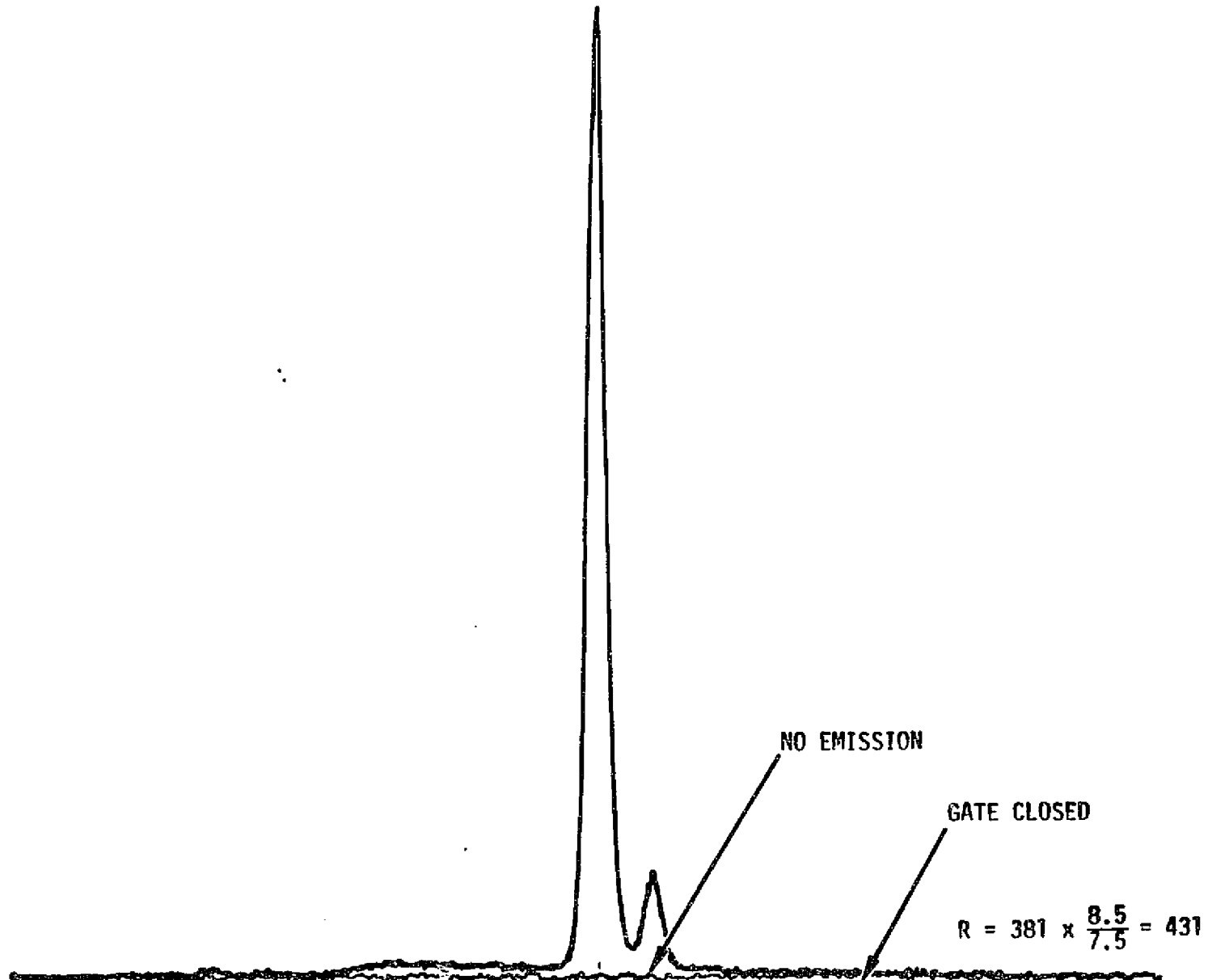
FIGURE 25

PFK With 0.001 Inch Slit-Before Modification

object slit width was 0.001 inch and the resolution obtained was 431. When the instrument was reassembled to increase the sensitivity of the apparatus the object slit width had been enlarged to 0.0023 inch. It was thought that an improvement in resolution would result in returning to a 0.001 inch. Since a resolution of 572 was already obtained with the 0.0023 inch slit it was questionable whether a significant improvement of resolution (with a concomitant decrease in sensitivity) would result in switching to the 0.001 inch slit. Project Note 6 looks at this question in detail, from the results, it was decided to leave the slit width at 0.0023 inch.

# 4. CONCLUSIONS

The experimental phase of this program showed that the conversion of the EI source to an EI/CI source was successful. Utilizing a two mil object slit, a resolution of 572 was obtained at m/e 381 in the EI mode. At the same time a resolution of 372 at m/e 180 was obtained in the CI mode. This compared to a resolution of 294 for the same peak in the EI mode.

The spectra generated by the chemical ionization did not exhibit the qualities that were expected. That is, the characteristic M + 1 peak (where M is the parent ion mass) was absent, nor was there a dramatic decrease in the number of lower mass peaks. The most likely reason for this behavior was the ratio of reagent to sample gas. This ratio under typical CI conditions should be $\geq 10^3$:1. Since our CI spectra were run at ratios less than this, we probably did not achieve complete chemical ionization conditions. As the gas handling system was designed for use with a GC this ratio could not be achieved in practice with steady state sample input.

The use of PFIA resulted in a distorted ion image; the actual image shape being very dependent on potential applied to the lens plates ahead of the MCA. The cause of this distortion needs to be determined, so that the advantages of using PFIA can be realized.

In general, the EI/CI capability of this instrument is very high. Some minor adjustments have to be made in the positioning of the magnet so that the maximized resolution can exist simultaneously along the entire ion focal plane. The instrument will then provide the type of analysis envisioned for it.

APPENDIX A

PROJECT NOTES

CONTRACT NAS7-100

Pumping System for CI/EI Source

Ion Source Gas Flows

Calculations of source conductance and data from the manufacturer show that
the required gas flow through the ion source is approximately 2 atm cc per min
of $CH_4$ to give a pressure of 0.5 torr in the ion source, or 4 atm cc per min
for pressure of 1 torr in the ion source. The pumping system for the ion
source housing should have sufficient speed to maintain a pressure of $1 \times 10^{-4}$
torr outside the ion source for 2 atm cc/min input of $CH_4$.

Gas input to the analyzer comes from two sources - source object slit and
leakage through the differential pumping carrier. Typically, these combined
gas flows will be in the range 1/2% to 1% of the gas flow to the ion source -
0.01 atm cc/min to 0.04 atm cc/min.

The pumping system for the analyzer must maintain pressure in the analyzer
below $1 \times 10^{-5}$ torr (preferably $5 \times 10^{-6}$ torr) to avoid broadening of the
mass peaks by ion-molecule collisions.

Source Pumping System

Desired pumping speed to maintain a pressure of $1 \times 10^{-4}$ torr for 2 atm cc/min
input of $CH_4$ is:

$$= \frac{2}{60} \cdot \frac{760}{10^{-4}} \cdot 10^{-3} \quad 1/sec$$

$$= 250 \ 1/sec$$

A Varian VHS-4 diffusion pump (1250 l/sec) and Varian 326-4 $LN_2$ trap (conductance 600 l/sec) had been previously selected for the source housing pumping system, yielding a combined speed of 405 l/sec for air or 543 l/sec for $CH_4$. Connection of the $LN_2$ trap to the source housing was planned as an elbow of 4 inches diameter with a design requirement that provision be made for possible later addition of a gate valve. This would increase the connection length to approximately 15 inches reducing the conductance of this line to 455 l/sec for $CH_4$ and the pumping speed at the ion source to 250 l/sec for $CH_4$.

The diffusion pump was backed by a Sargent-Welch 1402 mechanical pump with 150 l/min throughput in order to maintain low foreline pressures during CI operation.

Pumping speeds and pressures during CI operation are given in Figure 1.

Analyzer Pumping System

A Varian M2 diffusion pump (175 l/sec) and a Varian 325 $LN_2$ trap (conductance of 460 l/sec) had been previously selected for the analyzer pumping system, yielding a combined speed of 127 l/sec for air or 170 l/sec for $CH_4$.

The $CH_4$ gas input to the ion source and leakage from the source to the analyzer determines the required pumping speed at the analyzer. For 2 atm cc/min of $CH_4$ into the ion source and 1% leakage to the analyzer, the required pumping speed for an analyzer pressure of $5 \times 10^{-6}$ is:

$$= \frac{2}{60} \cdot 10^{-2} \cdot \frac{760}{5 \times 10^{-6}} \cdot 10^{-3} \ \text{l/sec}$$

$$= 50 \ \text{l/sec}$$

The only possible attachment point for the analyzer pumping system was to the source housing between the object slit and electric sector. Pumping line length to the $LN_2$ trap was approximately 18 inches because the $LN_2$ trap for

the analyzer system had to clear the components of the ion source pumping system. Conductance of the connecting line was computed for various diameters:

| Line Diameter | Conductance (1/sec) | |
| --- | --- | --- |
| | Air | CH4 |
| 2" | 35 | 47 |
| 2-1/2" | 69 | 92 |

A 2-1/2 inch tube was therefore used, which combined with the speed of 170 1/sec for pump and $LN_2$ trap would give a speed of 60 1/sec at the analyzer.

Pumping speeds and system pressures during CI operation are given in Figure 2.

| Components | Pumping Speed For $CH_4$ and for (air) | Pressure (Torr) 2 atm cc/min $CH_4$ Input |
|---|---|---|
| Ion Source | | 0.5 |
| Ion Source Housing | 250 l/sec (185) | $1 \times 10^{-4}$ |
| 4 inch OD Elbow | | |
| Possible Gate Valve | 543 l/sec (405) | |
| $LN_2$ Trap | 1675 l/sec (1250) | $1.5 \times 10^{-5}$ |
| VHS-4 Diffusion Pump | 160 l/min (160) | $10^{-2}$ |
| 1402 Forepump | | |

FIGURE 1

Ion Source Pumping System

| Components | Pumping Speed For $CH_4$ and For (air) | Pressure (Torr) 2 atm cc/min $CH_4$ 1% Leakage |
|---|---|---|
| Analyzer | | $5 \times 10^{-6}$ |
| | 60 (45) | |
| Connecting Line | | |
| Possible Gate Valve | | |
| | 170 (127) | |
| $LN_2$ Trap | | |
| | 235 1/sec (175) | $1.3 \times 10^{-6}$ |
| M2 Diffusion Pump | | |
| | 60 1/min (60) | $< 10^{-3}$ |
| 1405 Forepump | | |
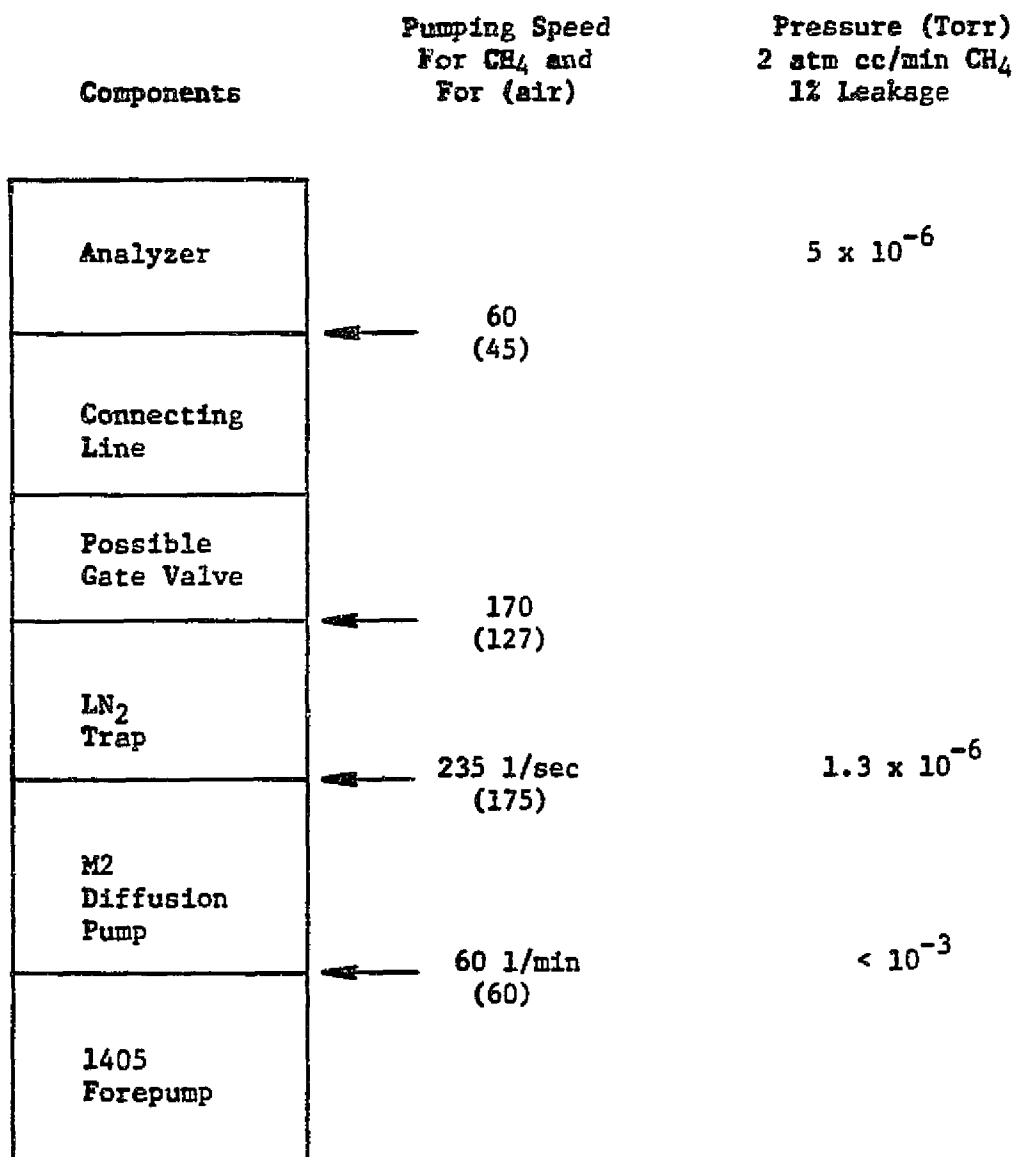
FIGURE 2

Analyzer Pumping System

## Ion Source Housing

The requirements for the ion source housing were:

1.  Maintain the design dimension of 3.640 inches between object slit and electric sector.
2.  Provide adequate pumping at the ion source.
3.  Provide adequate pumping to the analyzer region.
4.  Source to be easily removable for cleaning and maintenance.

The design finally chosen is shown in Figure 1. Previous calculations showed that a 2-1/2 inch OD pumping tube for the analyzer region was desirable, however it is not physically possible to connect a pumping line of this size in the space between the ion source and the flanges associated with the electric sector. The 2-1/2 inch line from the M2 diffusion pump was therefore attached to a 2-1/2 inch to 2 inch reducing cone for connection to the ion source housing. This will cause a small loss of pumping speed from the calculated value of 60 l/sec, but still yield a pumping speed in excess of the required value of 50 l/sec.
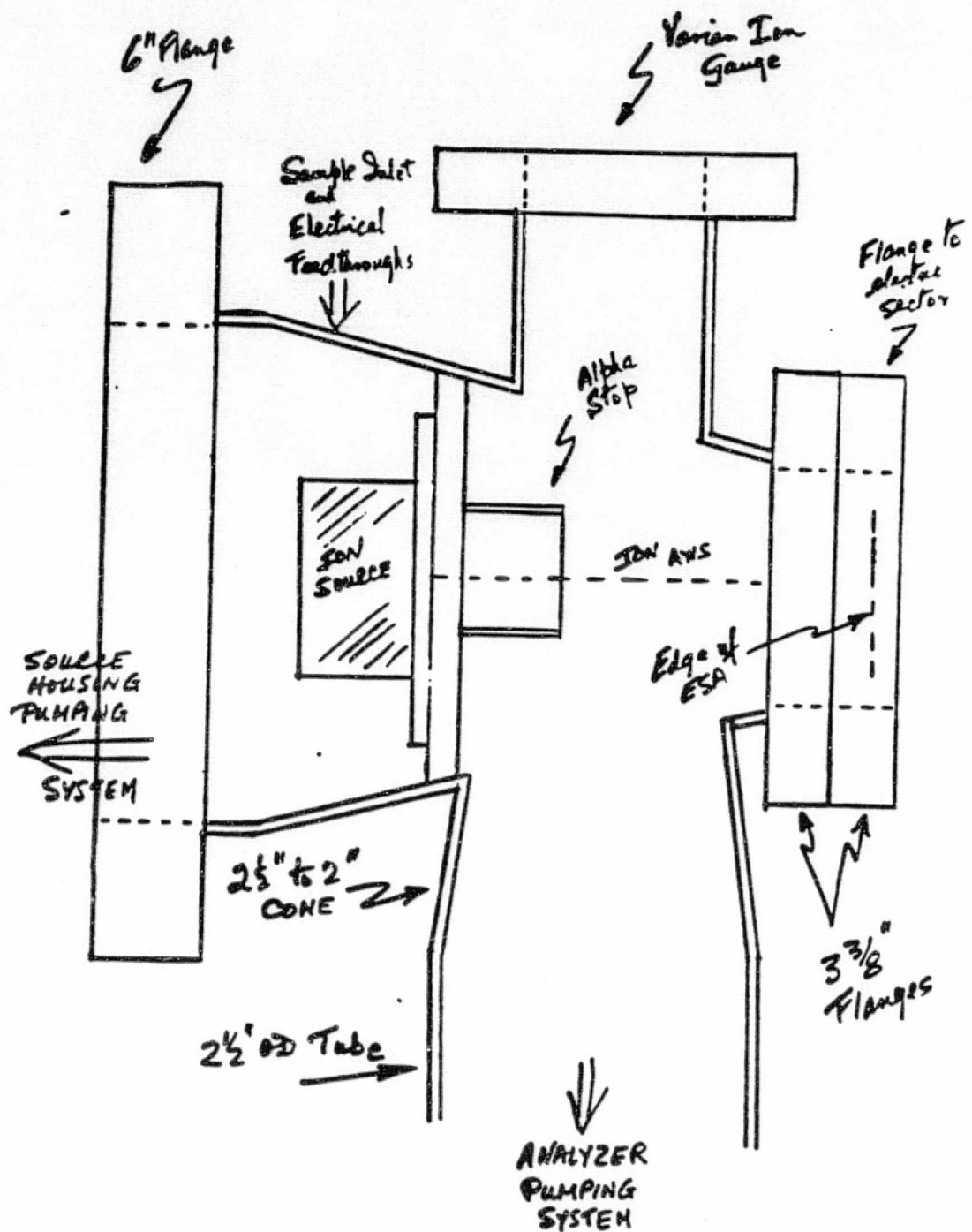
FIGURE 1

Cross-Section of Source Housing

## Calculation of Flow Rate Into Analyzer Region From Source Region Using PFB-2

To determine the flow rate from the source to the analyzer, it was decided to monitor the pressure changes in the source and analyzer regions while increasing the flow of PFB-2 through the inlet system.

The pumping speed in the source region is 250 1/sec and in the analyzer region it is 60 1/sec.

|  |  | Pressure (Torr) | $\Delta P$ (Torr) | $Q\ (\frac{\text{std-cc}}{\text{sec}})$ |
|---|---|---|---|---|
| Source | 1) | $3.4 \times 10^{-7}$ | -- | -- |
|  | 2) | $7.8 \times 10^{-6}$ | $7.46 \times 10^{-6}$ | $2.45 \times 10^{-3}$ |
|  | 3) | $4.9 \times 10^{-5}$ | $4.12 \times 10^{-5}$ | $1.36 \times 10^{-2}$ |
|  | 4) | $1.04 \times 10^{-4}$ | $5.5 \times 10^{-5}$ | $1.81 \times 10^{-2}$ |
| Analyzer | 1) | $2 \times 10^{-6}$ | -- | -- |
|  | 2) | $2 \times 10^{-6}$ | -- | -- |
|  | 3) | $2.9 \times 10^{-6}$ | $9 \times 10^{-7}$ | $7.11 \times 10^{-5}$ |
|  | 4) | $4.0 \times 10^{-6}$ | $1.1 \times 10^{-6}$ | $8.68 \times 10^{-5}$ |

The flow rate in the source region is calculated by the following relationship.

$$250\ \frac{\ell}{\text{sec}} \times 10^3\ \frac{\text{cc}}{\ell} \times \Delta P(\text{Torr}) \times \frac{1}{760}\ \frac{\text{std-cc}}{\text{Torr-cc}} = Q\ (\frac{\text{std cc}}{\text{sec}})$$

While the flow rate for the analyzer region is

$$60\ \frac{\ell}{\text{sec}} \times 10^3\ \frac{\text{cc}}{\ell} \times \Delta P(\text{Torr}) \times \frac{1}{760}\ \frac{\text{std-cc}}{\text{Torr-cc}} = Q\ (\frac{\text{std-cc}}{\text{sec}})$$

To determine the flow rate from source to analyzer one obtains Q' by the following relationship

$$Q' = \frac{\text{Flow Rate in Analyzer}}{\text{Flow Rate in Source}} \times 100$$

|     | Q' (%) |
|-----|--------|
| 1)  | --     |
| 2)  | --     |
| 3)  | 0.52   |
| 4)  | 0.48   |

Thus, the average flow rate from the source into the analyzer is 0.5%.

## Inlet System for CI, EI Source

An inlet system is designed to interface between a GC column and a CI, EI source for the JPL Focal Plane mass spectrometer.

The GC column will be WCOT with a flow rate of about 2 atm cc/min and where Methane will be used as a carrier gas. In the CI mode the carrier gas will also be used as the reagent gas.

The ion source conductance for Methane at $220^\circ$C is 34 cc/s in the molecular flow region and 57 cc/s in the critical flow region. The gold leak in the ion source inlet sample line has a conductance of 0.21 cc/sec for Methane at $220^\circ$C in the molecular flow region and 0.35 cc/sec in the critical flow region.

## CI Mode

In the CI mode the entire G.C. carrier gas can be allowed to flow into the source. The pressure in the ion source will be:

$$P = Q/C$$

where,
$$Q = 2 \text{ atm cc/min}$$
$$= 25.4 \text{ torr-cc/s}$$
$$C = 57 \text{ cc/s}$$
$$\therefore P_{source} = 0.44 \text{ torr}$$

In this pressure regime the mean free path will be much less than the source dimension and therefore the flow will be viscous out of the source.

The pressure upstream from the gold leak will be:

$$P = \frac{25.4 \text{ torr-cc/s}}{0.35 \text{ cc/s}}$$

$$= 72.6 \text{ Torr}$$

Therefore all that is necessary will be a line to connect the G.C. column to the ion source on the upstream side of the gold leak. The flow through this line will be 25.4 torr-cc/s with a pressure of 760 torr at the G.C. end and 72.6 torr at the source end. The dimensions of the line can now be evaluated using Poiseuille's equation.

$$Q = 1.553 \times 10^5 \ (P_1^2 - P_2^2) \ \frac{D^4}{L}$$

where, Q is the flow, $P_1$ and $P_2$ are the pressures at the ends of the line, D is the inner diameter and L is the length.

For Q = 25.4 torr-cc/s, $P_1$ = 760 torr, $P_2$ = 72.6 torr

$$\frac{D^4}{L} = 2.86 \times 10^{-10}$$

Therefore, if the I.D. of the line is chosen to be .006 inch then L = 188.8 cm.

The schematic of the flow would look as follows:
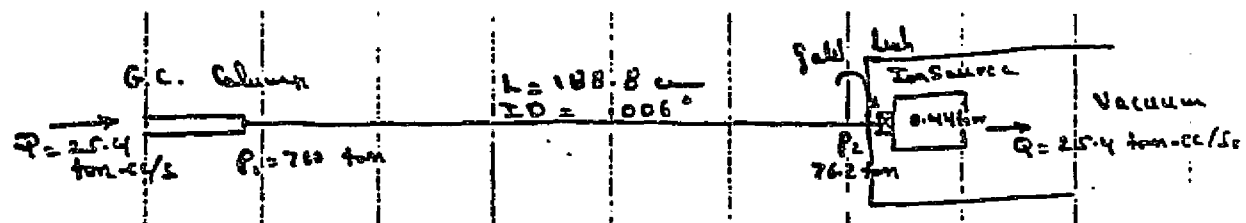


Therefore, choosing a 188.8 cm line with .006 inch I.D. will be sufficient for operation in the CI mode. Here, the entire carrier gas flow will be allowed to enter the ion source.

The time constant in this case will be the inner volume of the tube divided by the conductance of the gold leak

$$\tau = \frac{\frac{\pi}{4}(.006 \times 2.54)^2 \times 188.8}{0.35} \times \frac{\frac{2}{3}(P_1 - P_2)}{P_2} \div P_2$$

or,    $\tau = 0.70$ sec


This assumes no dead volume in the fittings.


## EI Mode


In the EI mode the source pressure must not exceed $10^{-4}$ torr which limits
the sample flow to a maximum of $3.4 \times 10^{-3}$ torr-cc/s. Therefore, most of the
25.4 torr-cc/sec flow from the GC must be pumped out ahead of the source.
Pumping this flow at the end of the GC line would be undesirable as it will
drop the pressure at that point and this in turn will change the pressure
distribution in the column. However, if another line is placed between the GC
and the point where the sample is being pumped, thus the column will terminate
at one atmosphere pressure and therefore not change its performance.


The flow lines will now look as follows:
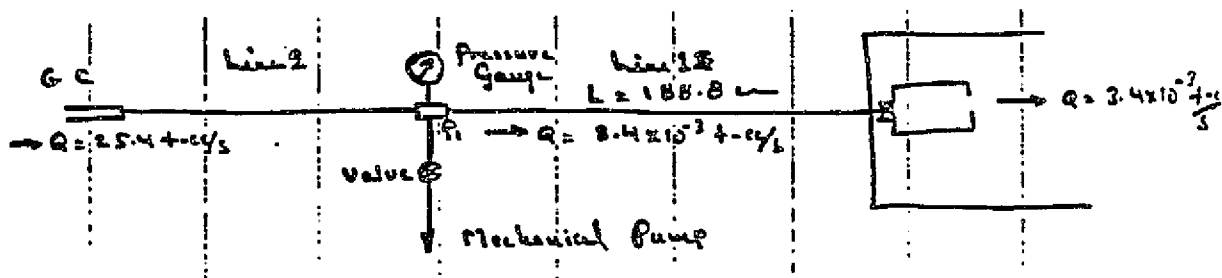


The dimensions of the line 1 were already derived in the CI section; L = 188.8 ccm
D = .006 inch. But now the flow is $3.4 \times 10^{-3}$ torr -cc/s and therefore the
pressure $P_1$ need be calculated.
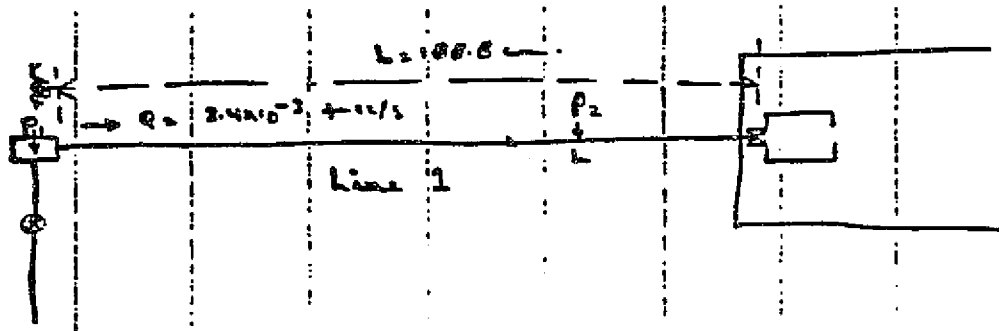
The flow at the beginning of the line will be viscous while near the ion source end it will be molecular.

Assuming $P_2$ is the pressure downstream in line 1 where the flow is viscous and where,

$$\lambda/D = 0.1 \qquad \lambda = \text{mean free path}$$

Or, $\qquad \lambda = .0015 \text{ cm}$

$$\lambda = \frac{5.09}{P(\mu)}$$

This corresponds to a pressure of 3.3 torr. Thus, if $P_2$ is 3.3 torr at some distance L, the $P_1$ and L are related by means of Poiseuille's equation

$$Q = 1.553 \times 10^5 \, (P_1{}^2 - P_2{}^2) \, \frac{D^4}{L}$$

which for $Q = 3.4 \times 10^{-3}$ t − cc/s, $P_2 = 3.3$ torr, $D = .015$ cm reduces to

$$L = 2.38 \, (P_1{}^2 - 10.89)$$

The following table gives values of L for different values of $P_1$:

| $P_1$ | L |
|-------|-------|
| 5 torr | 33.6 cm |
| 6 torr | 59.8 cm |
| 7 torr | 90.7 cm |
| 8 torr | 126.4 cm |
| 9 torr | 166.9 cm |

In other words, by varying the pressure $P_1$ one can vary the length of the tube over which the flow is viscous.

Pressure $P_1$ can be controlled by throttling the flow to the vacuum pump.

As far as line 2 is concerned its length and/or inner diameter will be determined strictly by the flow rate since $P_1$ is much less than an atmosphere. The flow will be viscous

$$Q = 1.553 \times 10^5 \ (P_0{}^2 - P_1{}^2) \ \frac{D^4}{L}$$

In this case $Q = 25.4$ torr-cc/sec, $P_0 = 760$ torr, $P_1{}^2 << P_0{}^2$

$$\therefore D^4 = 2.83 \times 10^{-10} \ L$$

Using GC line with $D = .006$ inch would require the line to be 190.5 cm long.
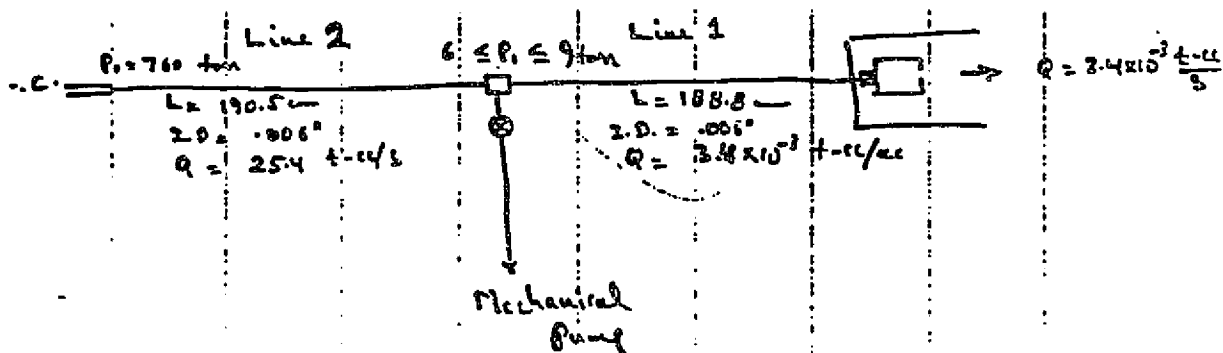


In the EI mode line 2 must be added to allow the GC column to terminate at 1 atmosphere pressure and to allow the pressure at the head of line 1 be a few torr which will restrict the flow to the MS and maintain the source pressure below $10^{-4}$ torr. In the CI mode line 2 must be removed.

Using the Valco 4 port valve or an equivalent, line 2 can be added between the GC column and line 1 for EI mode, or it can be removed for the CI mode.

Figure 1 gives a more detailed mechanical assembly of the inlet system with two different valve positions for CI and EI modes.

Line 2

1/16" O.D. x .006" I.D. SST G.C. TUBING
120 cm (74.80") TOT. LENGTH TO SCALE

1/4" O.D. x .028 WALL SST TUBING

VALCO ZERO VOLUME
TEE ZUT-06.2

1/16" O.D. x .006" I.D. SST
G.C. TUBING (MIN. LENGTH TO DISASSEMBLE)

VALCO 1/4" TO 1/16" ADAPTER
ZUTA-250/062

SWAGELOCK 1/4" FEMALE BRANCH TEE
SS-400-3 TTF

VALCO 4 PORT
ZERO VOLUME
VALVE CV-4-11/16

FROM
G.C.

1/16" TUBE 1 FOOT
G.C. (TOT. LENGTH)

CI Mole

B.I. Mole

GRANVILLE-PHILLIPS
GAGE TUBE
(SEE GFE LIST)
1/8" NPT REF.

SWAGELOCK 1/4"
BELLOWS VALVE
BN-4HK

Line 1

1/16" O.D. x .006" I.D. SST
G.C. TUBING
1885 cm (72.0") TOT.
LENGTH TO SCALE

SWAGELOCK 1/4" PORT
CONNECTER
SS-401-PC

OR 1/4" O.D. x .028" WALL
SST TUBING
TO SUIT

VALCO ZERO DEAD
VOLUME 1/16" UNION
ZVU-062

TO
ROUGHING
PUMP

ION
SOURCE

VALVE POSITIONED FOR 375 cm INLET LOOP
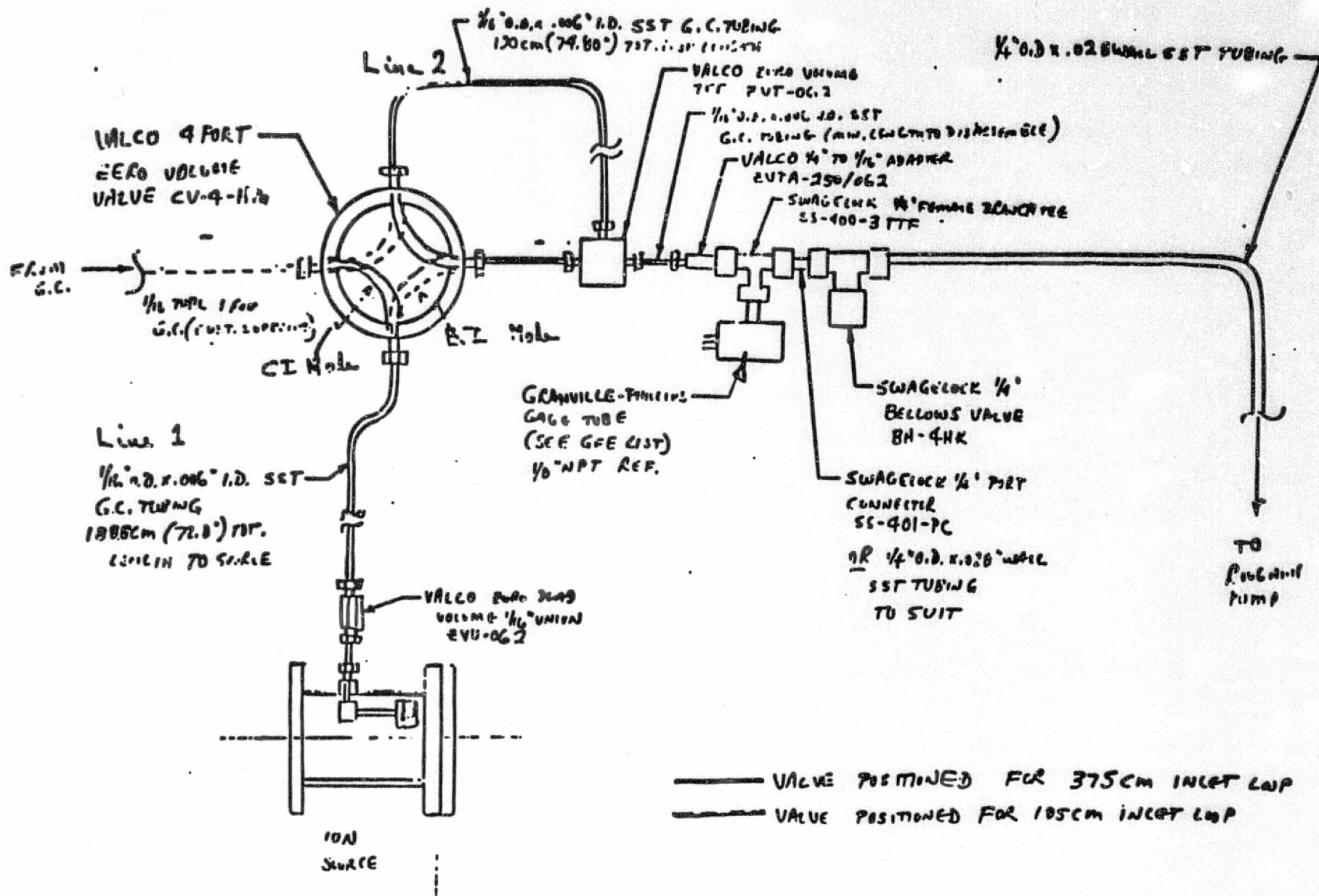
VALVE POSITIONED FOR 105 cm INLET LOOP

FIGURE 1

Inlet System

## Evaluation of the GC/EI Inlet System

In this project, a capillary GC column will be used with a flow rate of approximately 2 atm cc/min. When operating in chemical ionization mode (CI), methane will be used as the carrier gas as well as the reagent gas. In order to optimize the CI process, a pressure of 0.5 to 1 torr should be maintained in the ion source. For this instrument, a DuPont ion source is employed. Since the ion source is held at 1300 volts, the discharge phenomenom between the source block and the grounded GC inlet should be considered.

In the original DuPont design, a gold leak in the inlet line was used to maintain a much higher pressure (> 50 torr) at the upstream from the gold leak. This arrangement needs a long restriction line between the GC end and the gold leak to maintain such a pressure. This design will result in a time constant and a possibility of broadening the peak. An alternative design is to remove the gold leak and place an insulated tubing between the inlet line and the source block. In the present system, a 5 cm long, 1.55 mm I.D. Vespel tube is employed. To test the adequacy of this arrangement, a simulated system to study the discharge characteristic is shown in Figure 1.

Pressure inside the discharge tube is controlled by the regulator, needle valve, and the throttle valve. To carry on the experiment, a certain pressure was set first. The voltage applied to the anode was then increased until a visible discharge was maintained. A plot of the discharge voltage as a function of pd for different d is shown in Figure 2, where p is the pressure in torr and d is the length in cm. Figure 3 shows a similar plot where d is fixed at 5 cm and tubes with different I.D. were employed. The discharge current in both cases is from 0.2 mA to 0.8 mA.

The sparking potential and the values of V/pd are determined by the total number of molecules which an electron encounters in a linear path across the

gap. Figure 3 demonstrates that when the I.D. of the discharge tube is reduced, the number of gas molecules in the tube decreases, hence a higher voltage is required to initiate the discharge.

In summary, the present experiment demonstrates that the design of the inlet connection using a 5 cm long, 1.55 mm I.D. Vespel tube, is adequate. Should a higher voltage be used in a similar design, the I.D. of the tube can always be reduced to achieve the purpose.
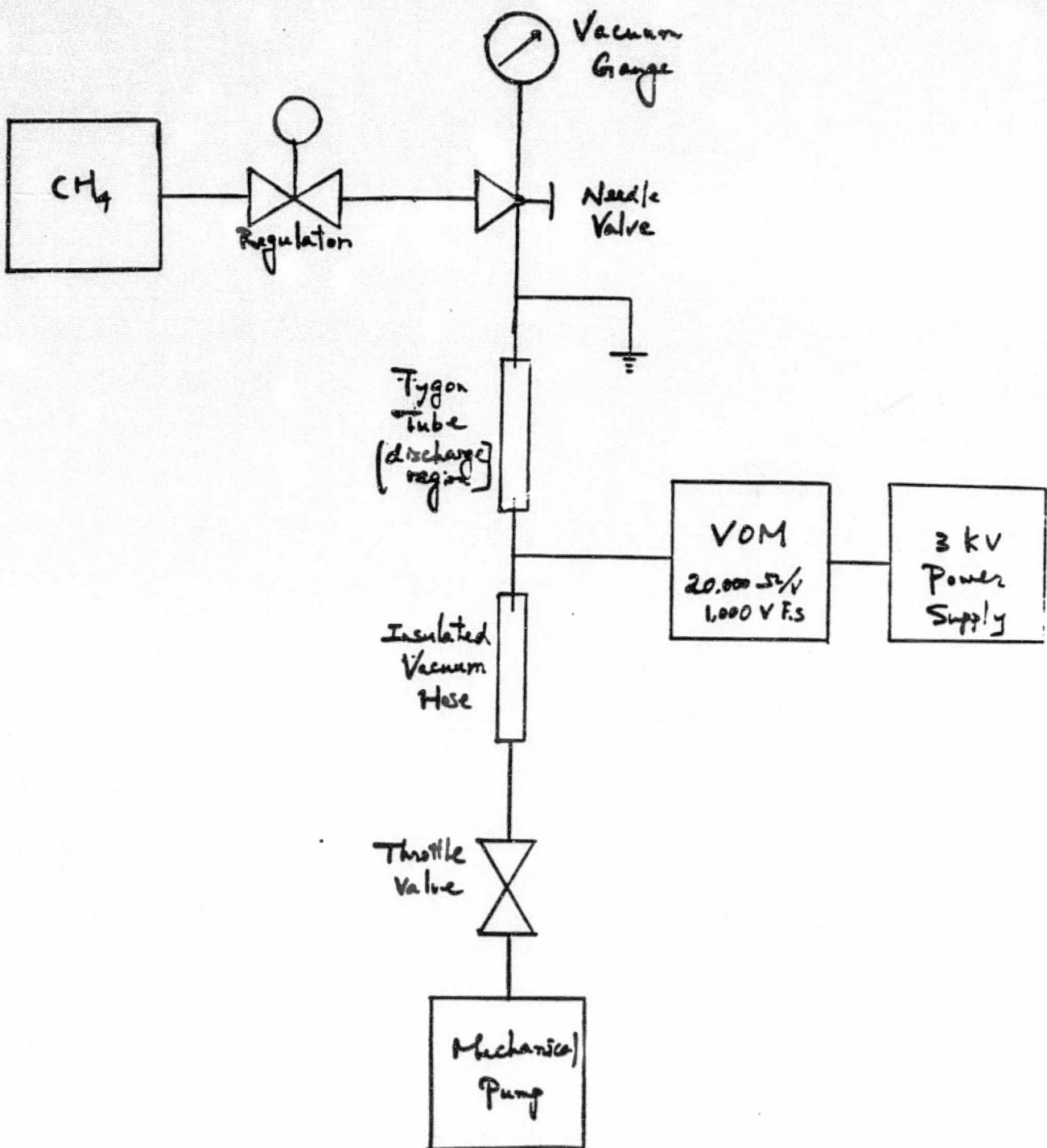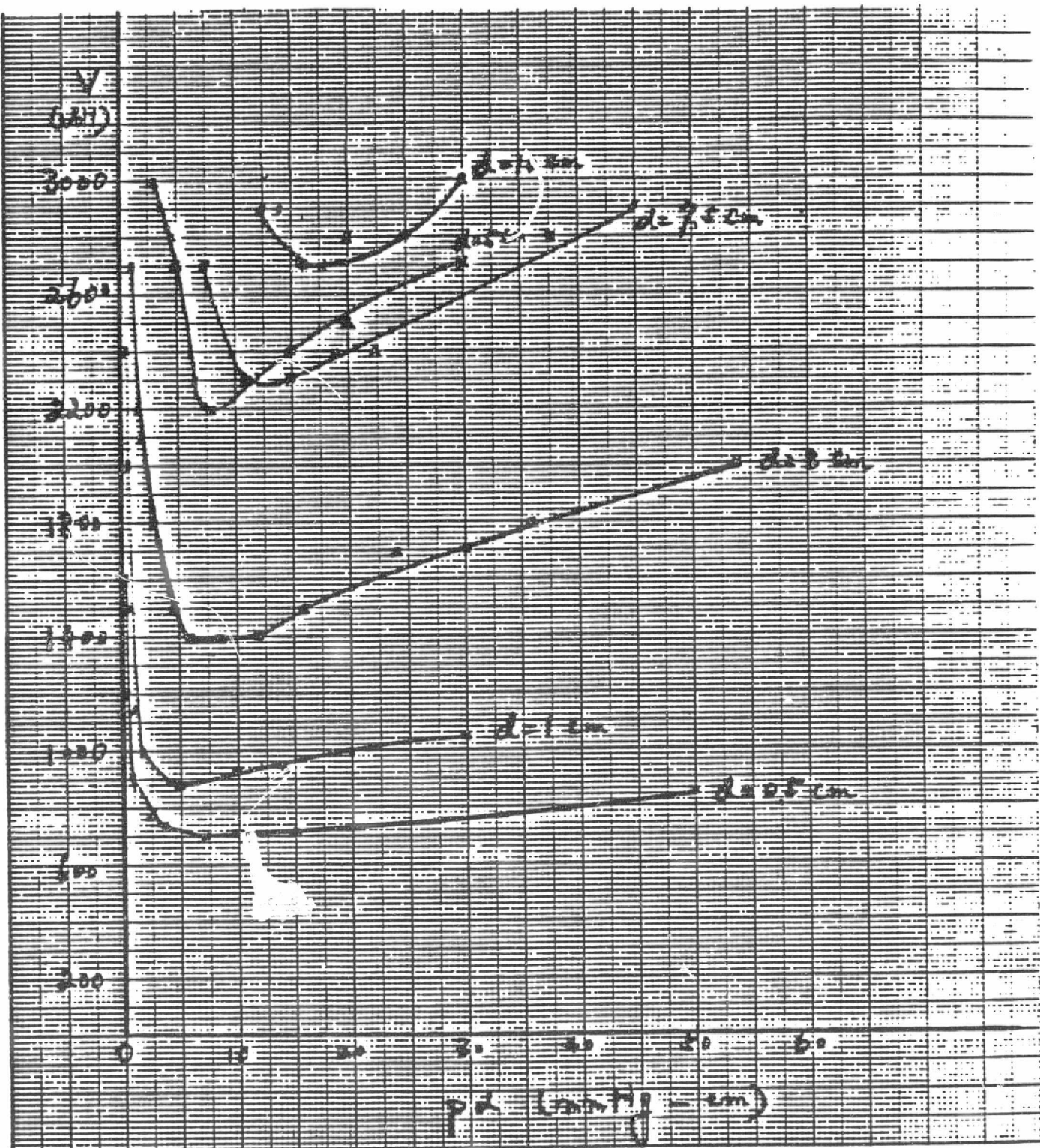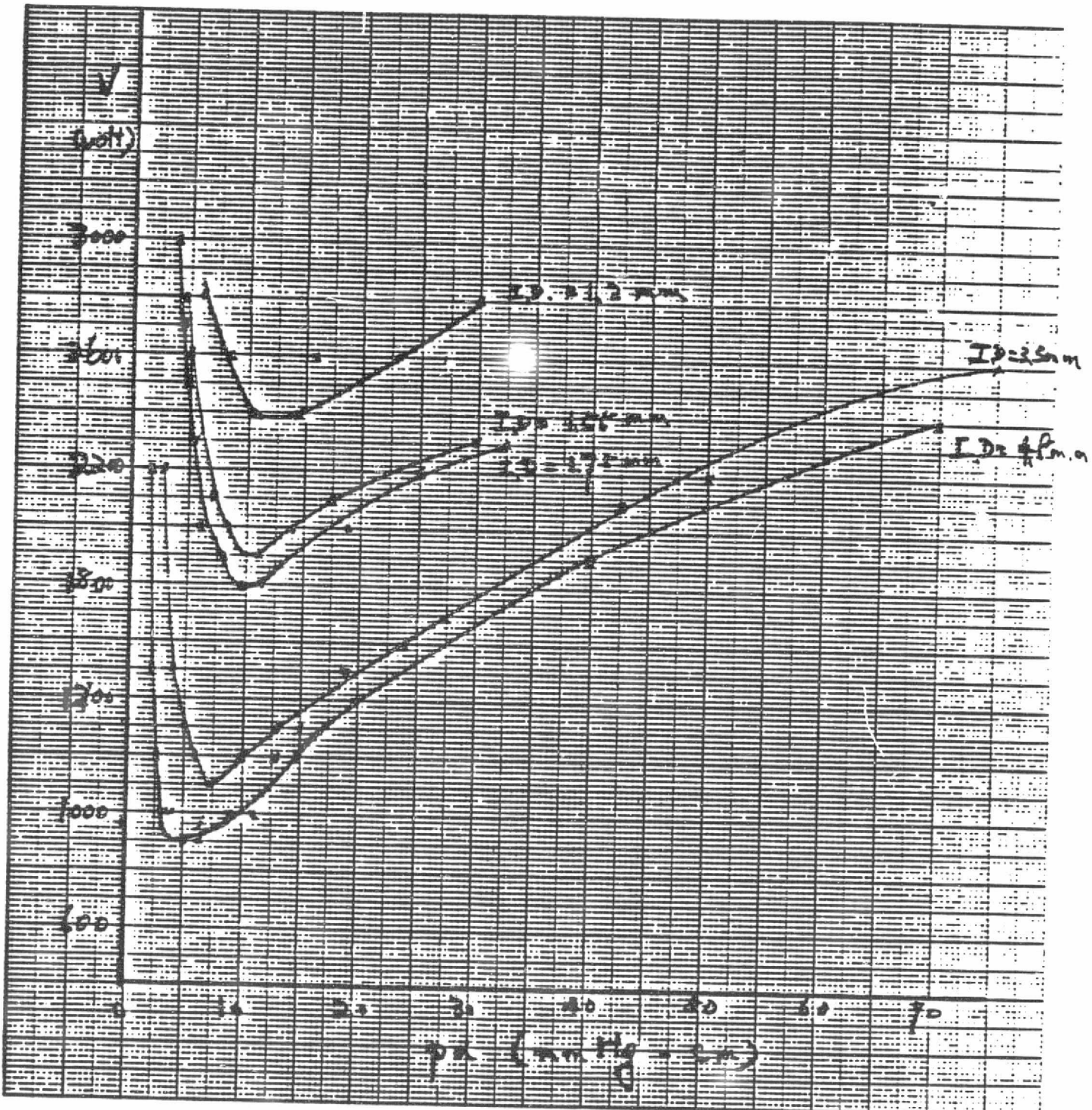
FIGURE 1

FIGURE 2

FIGURE 3

## Calculation of Theoretical Resolution of Spectrograph

Expression for overall beam width (b) in terms of aberrations

$$b = M_m S_o + r_m B_{11} \alpha^2 + 2r_m B_{12} \alpha\beta + \frac{z^2}{2r_m} + r_m A_\theta$$

$$+ 0.05 \, r_m \, z^2 + .00059 + .00100$$

where:

$M_m$ = demagnification of slit

$B_{11}$ = $\alpha^2$ aberration coefficient of Robinson

$B_{12}$ = $\alpha\beta$ aberration coefficient

$z^2/2r_m$ = Berry Curvature

$A_\theta$ = aberration due to tilted detector

$.05 \, r_m z^2$ = Z-focus einzel aberration

$.00059$ = channel width of MCA

$.00100$ = detector width

Requirements:

Unity mass resolution at m/e 500 or $\Delta m = 0.5$ amu at m/e 250 ($r_m = 3"$)

$$B_{11} = -1.416 + \frac{\gamma}{2} \left(\frac{r_e}{r_m}\right)^2$$

$r_e$ = electric sector radius

$r_m$ = magnetic sector radius

$\gamma$ = 1 for flat magnet pole faces

$B_{11} \to 0$ choosing appropriate value of $r_e/r_m$

Setting $B_{11} = 0$

$$\frac{1}{2}\left(\frac{r_e}{r_m}\right)^2 = 1.416 \qquad\qquad \frac{r_e}{r_m} = 1.683$$

$$B_{12} = 3.22 + \frac{r_e}{r_m} + \frac{r_e}{r_m}\left(.293\,\frac{r_e}{r_m} + \frac{d}{r_m}\right)$$

d = separation between faces of electric and magnetic sectors = 4.0"

## Berry Curvature $\qquad\qquad z^2/2r_m$

Z = half height of beam = 0.050"; $r_m$ = 3"

$$\frac{z^2}{2r_m} = \frac{25 \times 10^{-4}}{2 \times 3} = 0.00042 \text{ for } r_m = 3"$$
$$0.00063 \qquad r_m = 2"$$
$$0.00032 \qquad r_m = 4"$$

## $A_\gamma$ Term

$$A_\theta = 2\,\alpha Z\,\frac{r_e}{r_m^2}\,\sin\theta \qquad\qquad \theta = 20°$$

$$\alpha = 1.7 \times 10^{-2} \text{ radians}$$

$$Z = 0.050"$$

$$A_\theta = \frac{2.94 \times 10^{-3}}{r_m^2} = \qquad\qquad .00074 \text{ for } r_m = 2"$$
$$.00033 \text{ for } r_m = 3"$$
$$.00018 \text{ for } r_m = 4"$$

$0.05\,r_m Z^2$ – Z-focus Einzel Aberration

$$= 0.00038 \text{ for } r_m = 3"$$

## Magnification

$$M_m = \frac{r_m}{r_e} = .594 \text{ for } r_m = 3"$$

## $B_{12}$ term

$$B_{12} = 3.22 \div 1.68 + 1.68 \,(.293 \times 1.68 + 1.333)$$

$$B_{12} = 7.996$$

$$2r_m \, B_{12} \, \alpha\beta = 2 \times 3.0 \times 7.996 \times \underbrace{\left(1.74 \times 10^{-2}\right)}_{\alpha} \times \underbrace{\left(1 \times 10^{-3}\right)}_{\beta} = 8.35 \times 10^{-4}$$

$$B_{12} \,(r_m = 4) = 6.24$$

$$B_{12} \,(r_m = 2) = 12.69$$

$$2r_m \, B_{12} \, \alpha\beta = 2 \times 4 \times 6.24 \times 1.7 \times 10^{-2} \times 10^{-3} = .00085 \,(r_m = 4)$$

$$= 2 \times 2 \times 12.69 \times 1.7 \times 10^{-2} \times 10^{-3} = .00086 \,(r_m = 2)$$

## $B_{11}$ term

$$B_{11} = -1.416 + 1/2 \,(r_e/r_m)^2$$

$$B_{11}/r_m = 4 = -1.416 + 1/2 \,(5.05/4.0)^2 = -0.619$$

## $r_m \, B_{11} \, \alpha^2$

$$-4.0 \times .619 \,(1.7 \times 10^{-2})^2 = -7.15_6 \times 10^{-4} \text{ in} \quad \text{for } r_m = 4''$$

$$r_m = 2''$$

$$r_m \, B_{11} \, \alpha^2 = 2.0 \times 1.772 \times 1.7_2 \times 10^{-4} = .00102$$

Comparison of various aberration terms and calculation of resolving power.

I. Slit width .0023

| $r_m \rightarrow$ | | 2" | 3" | 4" |
|---|---|---|---|---|
| 1. Magnification of slit $M_m S_o$ | | .00100 | .00140 | .00180 |
| 2. $\alpha^2$ coefficient of Robinson $\quad r_m B_{11} \alpha^2$ | | .00102 | .0 | -.00072 |
| 3. $\alpha\beta$ aberration $\quad 2r_m B_{12} \alpha\beta$ | | .00086 | .00084 | .00085 |
| 4. Berry curvature $\quad z^2/2r_m$ | | .00063 | .00042 | .00032 |
| 5. Aberration due to tilted detector $\quad r_m A_\theta$ | | .00148 | .00099 | .00072 |
| 6. Z-focus einzel aberration $.05 \, r_m z^2$ | | .00025 | .00038 | .00050 |
| Sum 1 through 6 | | .00524 | .00403 | .00347 |
| Correction due to tilted detector $\times 1/COSW$ | | .00741 | .00570 | .00491 |
| + Channel without MCA | | .00059 | .00059 | .00059 |
| Beam width in focal plane | | .00800 | .00629 | .00550 |
| + Detector width | | .00100 | .00100 | .00100 |
| Resolving power $\dfrac{M}{\Delta M} = \dfrac{\Delta m \, (r_m/2)}{(\Delta X) \, COSW}$ | | 157 | 291 | 435 |
| Resolving power $\bar{c}$ zero detector width | | 177 | 337 | 514 |
| Improvement in reducing detector width | | 13% | 16% | 18% |

II.  .0011" Slit

1.  $M_m S_o$                          .00044        .00065        .00087

| | | | |
|---|---|---|---|
| 1.  $M_m S_o$ | .00044 | .00065 | .00087 |
| $\Sigma$ (1) − (6) | .00468 | .00326 | .00254 |
| x 1/COSW | .00662 | .00464 | .00359 |
| ÷ MCA width | .00059 | .00059 | .00059 |
| Beam width in f.p. | .00721 | .00523 | .00418 |
| + Detector width | .001 | .001 | .001 |
| | .0082 | .0062 | .0052 |
| M/ΔM | 172 | 341 | 546 |
| M/ΔM c̄ Zero detector width | 196 | 406 | 677 |
| Improvement | 14% | 19% | 24% |

Conclusions

1.  Halving the slit width reduces the sensitivity by a factor of two but only results in a nominal improvement of resolving power.

2.  The $\alpha\beta$ aberration is nearly equal to the slit width times the magnification at 2" and nearly 50% of the latter at 4".  It gives the major contribution to the beam width at $r_m = 2"$.

3.  The resolution increases rapidly from $r_m = 2"$ to $r_m = 3"$ then begins to level off after $r_m = 4"$.